Electronic Supplementary Material (ESI) for Dalton Transactions.

Supporting Information

A Luminescent Cationic MOF for Bimodal Recognition of Chromium and Arsenic based Oxo-anions in Water

Subhajit Dutta,[†] [a] Sumanta Let, [†] [a] Mandar M. Shirolkar,[b] Aamod V. Desai,[a] Partha Samanta,[a] Sahel Fajal,[a] Yogeshwar D. More,[a] Sujit K. Ghosh*[a]

[a] Department of Chemistry, Indian Institute of Science Education and Research (IISER), Dr. Homi Bhabha Road, Pashan, Pune411008, India.

E-mail: *sghosh@iiserpune.ac.in* ***Tel:****91-20-25908076*

[b] Symbiosis Center for Nanoscience and Nanotechnology (SCNN), Symbiosis International (Deemed University) (SIU), Lavale, Pune 412115, Maharashtra, India.

[†] These authors contributed equally to this work.

Experimental Section:

Physical measurements:

Powder X-ray diffraction (PXRD) patterns were acquired from a Bruker D8 Advanced X-ray diffractometer in a 5° to 40° 2θ range by using Cu Kα radiation ($\lambda = 1.5406$ Å) with a scan speed of 0.9° min^{-1}. The Fourier transform infrared spectra (FT-IR) spectra were collected from Bruker spectrometer. The fluorescence spectroscopic studies were performed with Jobin Yvon Fluoromax-4 spectrofluorometer. The thermogravimetric analysis (TGA) were collected from a TGA analyzer (Perkin-Elmer STA6000) under N_2 atmosphere keeping the heating rate constant at 10 °C min^{-1}. The field emission scanning electron microscopy (FESEM) studies and energy dispersive X-ray (EDX) analysis data were acquired from a FEI Quanta 3D dual beam ESEM. The fluorescence imaging experiments were performed on Leica DM6B EPI-Fluorescence instrument.

X-ray structural studies

Single-crystal X-ray data of iMOF-4C was acquired at 150 K from Bruker D8 Venture Duo X-ray diffractometer equipped with a Microfocus X-ray source (operated at 50 W; 50 kV/1 mA) and graded multilayer optics for monochromatic Mo Kα radiation ($\lambda = 0.71073$ Å) with a focused X-ray beam and a Photon 100 CMOS chip based detector system. The crystal was mounted on nylon CryoLoops (Hampton Research) with Paraton-N (Hampton Research). The data integration and reduction were processed with SAINT software.[1] A multi-scan absorption correction was applied to the collected reflections.[2] The structure was solved by a direct method using SHELXTL[3,4] and was refined on F^2 with a full-matrix least-squares technique using the SHELXL-2014/7 [5] program package within the WINGX [6] programme. All of the hydrogen atoms were refined anisotropically. All of the hydrogen atoms were located in successive difference Fourier maps and they were treated as riding atoms using SHELXL default parameters. The structures were examined using the Adsym subroutine in PLATON to assure that no additional symmetries could be applied to the models. The SQUEEZE option[7] was used to eliminate the contribution from the disordered guest molecules. CCDC number: 2073931 for iMOF-4C contains the supplementary crystallographic data for this paper.

Analyte preparation:

First, stock solutions of all the anions were prepared from their respective sodium and potassium salts in water of concentration 0.5mM. Cr(VI) and As(V & III) based anion solutions were further diluted 10 times to prepare 0.05mM stock solution in water.

Titration with $CrO_4{}^{2-}$, $Cr_2O_7{}^{2-}$, $HAsO_4{}^{2-}$, $HAsO_3{}^{2-}$ and other competing anions with iMOF-4C:

1mg desolvated iMOF-4C was taken in a cuvette and 2mL water has been added to that. Initial luminescence spectra of iMOF-4C in water has been recorded by exciting at 330nm (spectra recorded in the range of 350-650nm). Then to the dispersed MOF in water, we have added stock solution of Cr(VI) ions in water (20µL to 200µL) and spectra were for each addition. With each addition of Cr(VI) anion, we found quenching in the fluorescence emission of iMOF-4C. Similar procedure was followed for titration of As(V) and As(III) based oxo-anions. With each addition of As(V) and As(III) anions, we found enhancement in the fluorescence emission of iMOF-4C individually. For competing studies, we have taken $SO_4{}^{2-}$, Cl^-, Br^-, $ClO_4{}^-$, $NO_3{}^-$ and SCN^- ions in water. In a typical way, for initial study we have taken 1mg of iMOF-4C in 2mL of water. To the dispersed MOF we have added 200µL of the competing anion from the stock solution and recorded the corresponding spectra to check the response of MOF towards other anions (which we have provided in a bar diagram profile). Later, in a similar way to the dispersed MOF (1mg) in water medium (2mL) we have added 200µL of competing anions and followed by the addition of 200µL individual oxo-anionic solutions from the stock as prepared earlier. We have recorded both responses of MOF in presence of competing anions and in presence of both competing anions and respective oxo-anions. By combining two responses, we got the sensitivity of iMOF-4C towards these oxo-anions in presence of other competing anions.

Detection Limit Calculation:

For calculating detection limit, Cr(VI), As(V) and As(III) (20 – 200µL, 0.05mM stock solutions) were added to probe (desolvated iMOF-4C) (1mg, in 2mL water) and fluorescent intensity was recorded. By plotting fluorescence intensity with increasing concentration of the oxo-anions, slope (m) of graph were calculated from there. Further, the standard deviation (σ) was calculated from five blank measurements of probe. Detection limit is calculated according to the formula:[8]

$$\textbf{Detection limit: } (3\sigma / m)$$

Oxo-anion capture study:

iMOF-4C (1mg) was immersed in an 2mL aqueous solution of 0.5mM $CrO_4{}^{2-}$ and subsequently UV-Vis absorbance spectra were recorded with different time intervals. Further, the percentage removal of the oxo-anion and decrement in concentration was calculated by using the following equation:

$$D_t = \frac{C_0 - C_t}{C_0} \text{ x } 100\% = \frac{A_0 - A_t}{A_0} \text{ x } 100\%$$

Where, D_t is the exchange capacity, C_0 and A_0 are initial concentration and absorbance of the oxo-anion solution respectively, C_t and A_t, are concentration and absorbance of the oxo-anion solution at specific times respectively.

Figures:

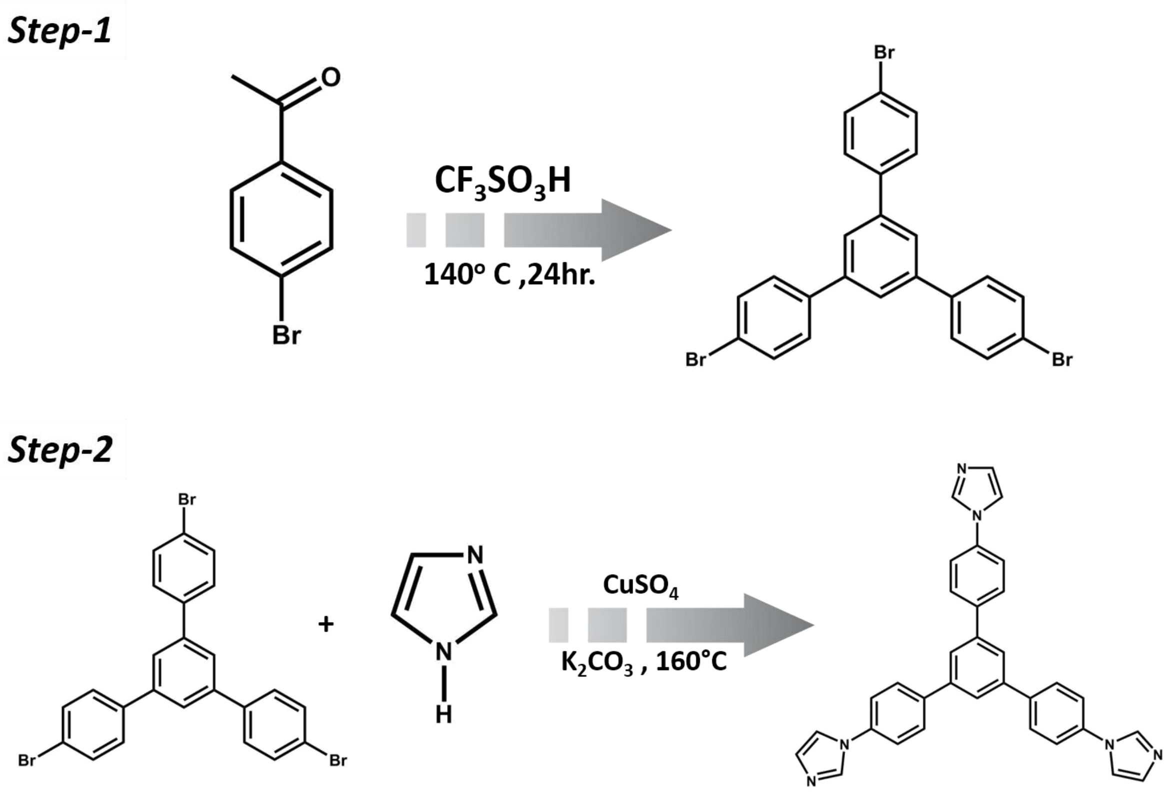

Scheme S1: Representation of the protocol employed for the synthesis of ligand (L).

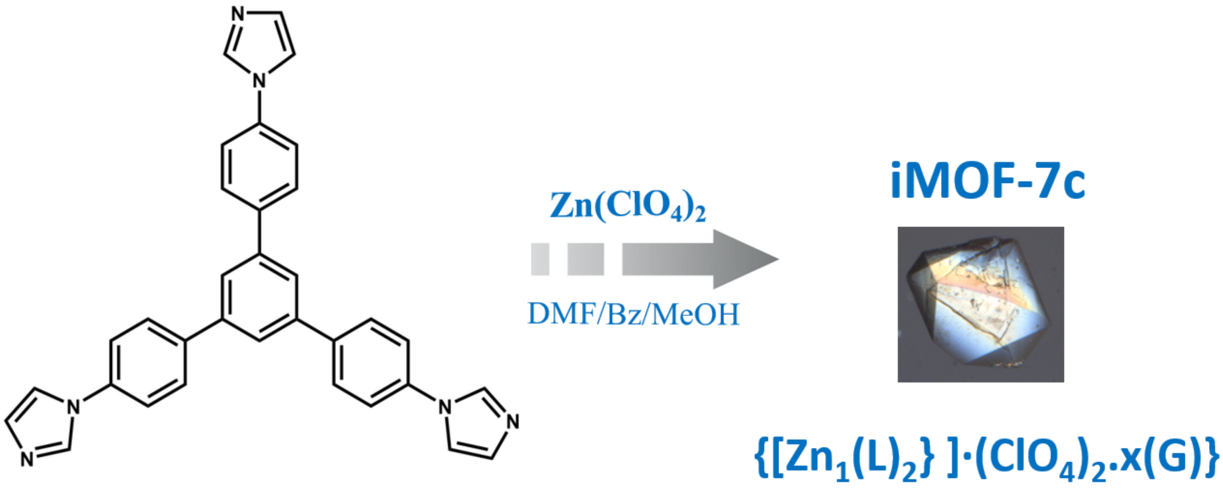

Scheme S2: Representation of the protocol employed for the synthesis of iMOF-4C.

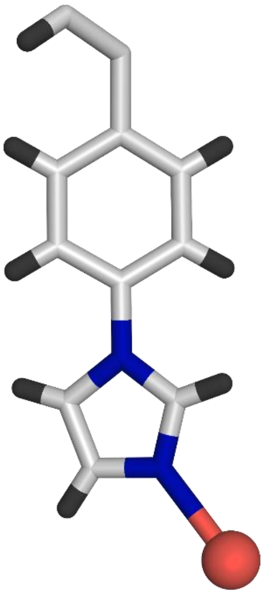

Figure S1: Asymmetric unit of iMOF-4C (Hydrogen atoms have been omitted for clarity, (color: Gray - C, Blue - N, Maroon - Zn), ClO_4^- anions have been omitted because of crystallographic disorder and clarity.

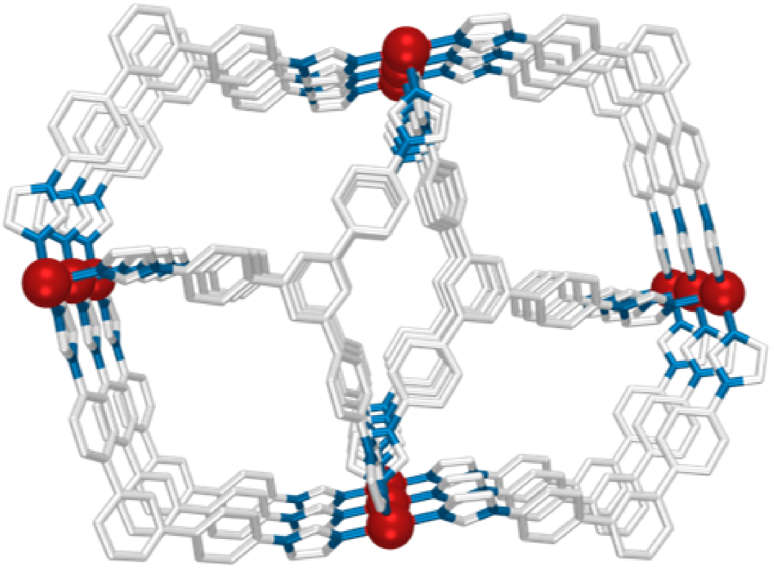

Figure S2: Coordination environment of iMOF-4C (Hydrogen atoms have been omitted for clarity, (color: Gray - C, Blue - N, Red - Zn).

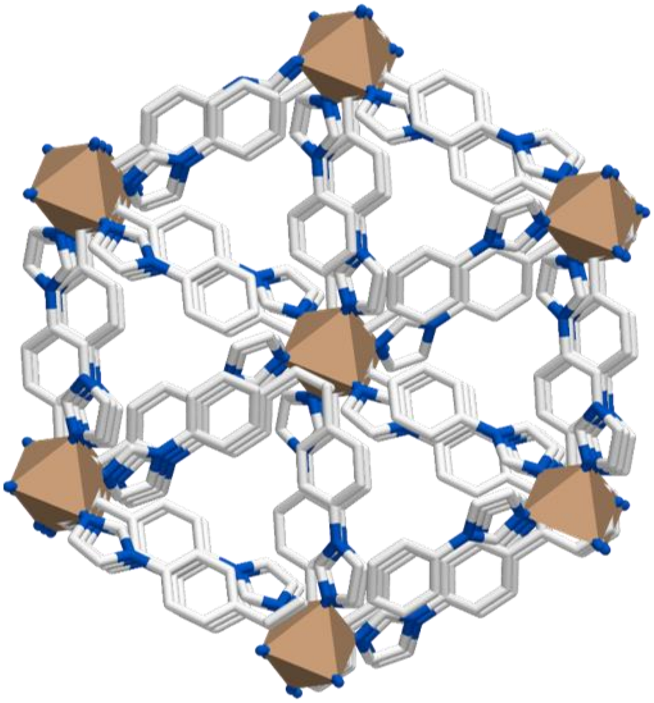

Figure S3: Orthographic view of overall packing of iMOF-4C. (Hydrogen atoms have been omitted for clarity, (color: Gray - C, Blue - N, Brown - Zn), ClO_4^- anions have been omitted because of crystallographic disorder and clarity.

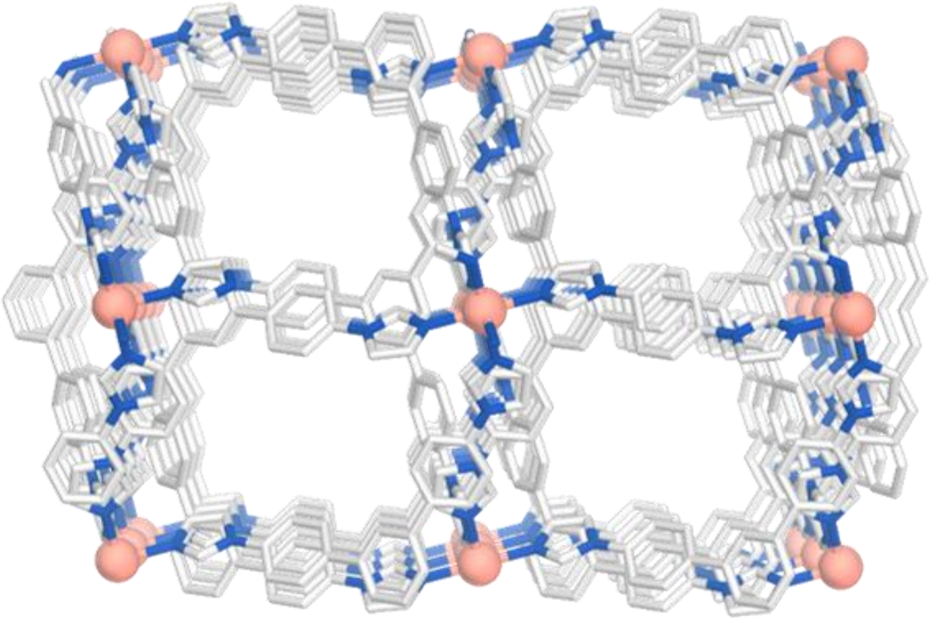

Figure S4: Perspective view of overall packing of iMOF-4C along c-axis. (Hydrogen atoms have been omitted for clarity, (color: Gray - C, Blue - N, Red - Zn), ClO_4^- anions have been omitted because of crystallographic disorder and clarity.

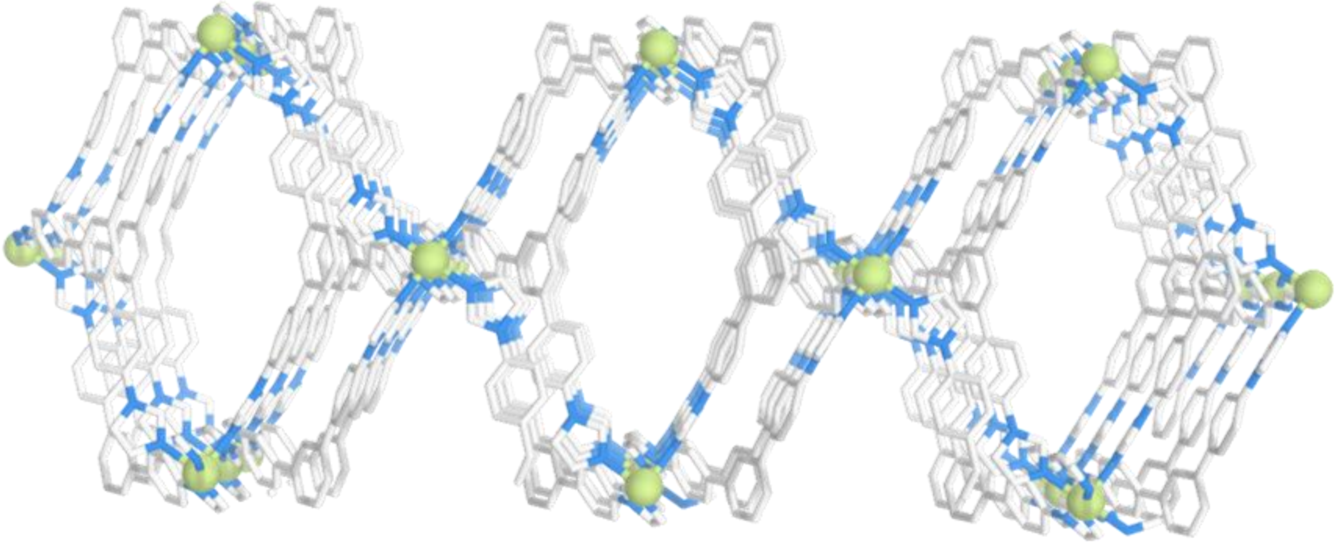

Figure S5: Perspective view of overall packing of iMOF-4C along c-axis. (Hydrogen atoms have been omitted for clarity, (color: Gray - C, Blue - N, Green - Zn), ClO_4^- anions have been omitted because of crystallographic disorder and clarity.

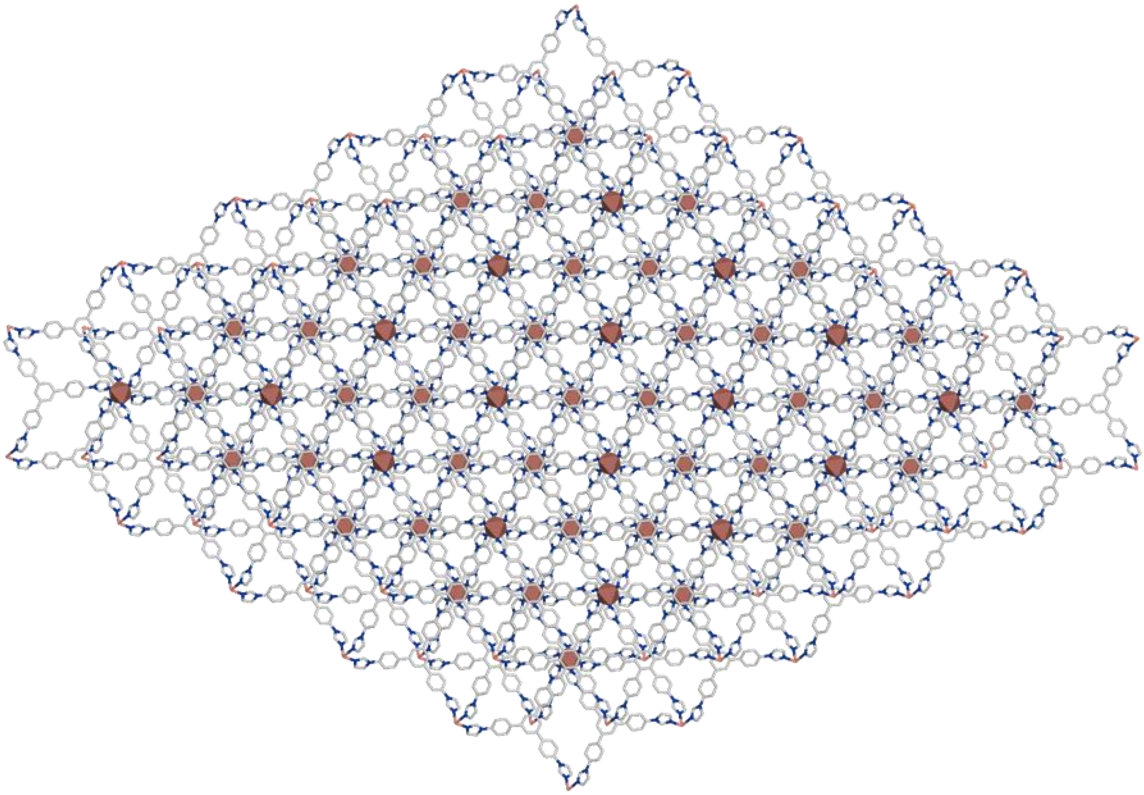

Figure S6: Orthographic view of overall packing of iMOF-4C. (Hydrogen atoms have been omitted for clarity, (color: Gray - C, Blue - N, Brown - Zn), ClO_4^- anions have been omitted because of crystallographic disorder and clarity.

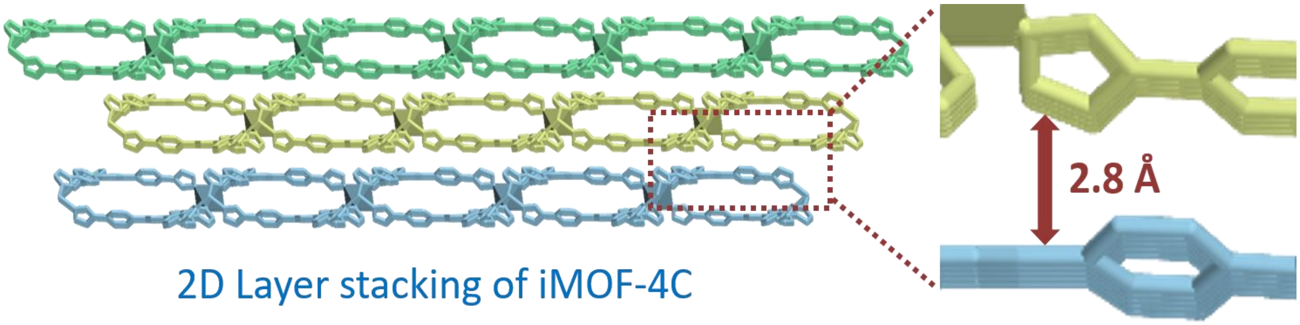

Figure S7: Packing diagram of iMOF-4C showing the distance between successive two 2D layers.

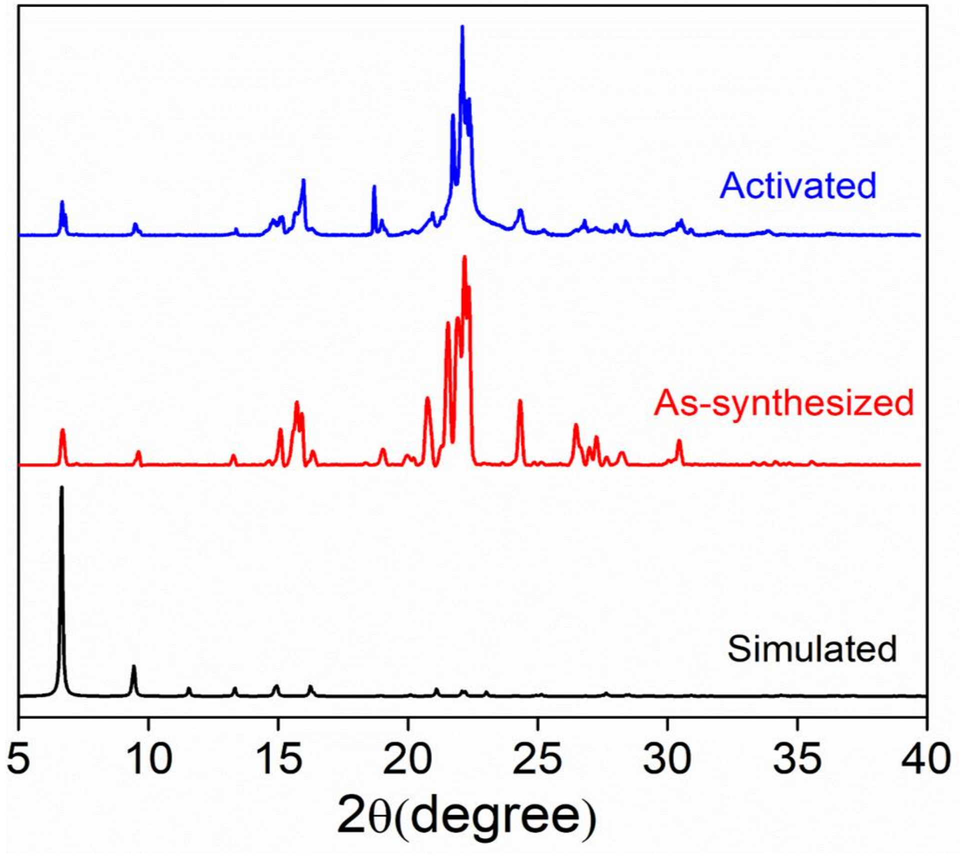

Figure S8: Powder X-ray diffraction patterns of iMOF-4C.

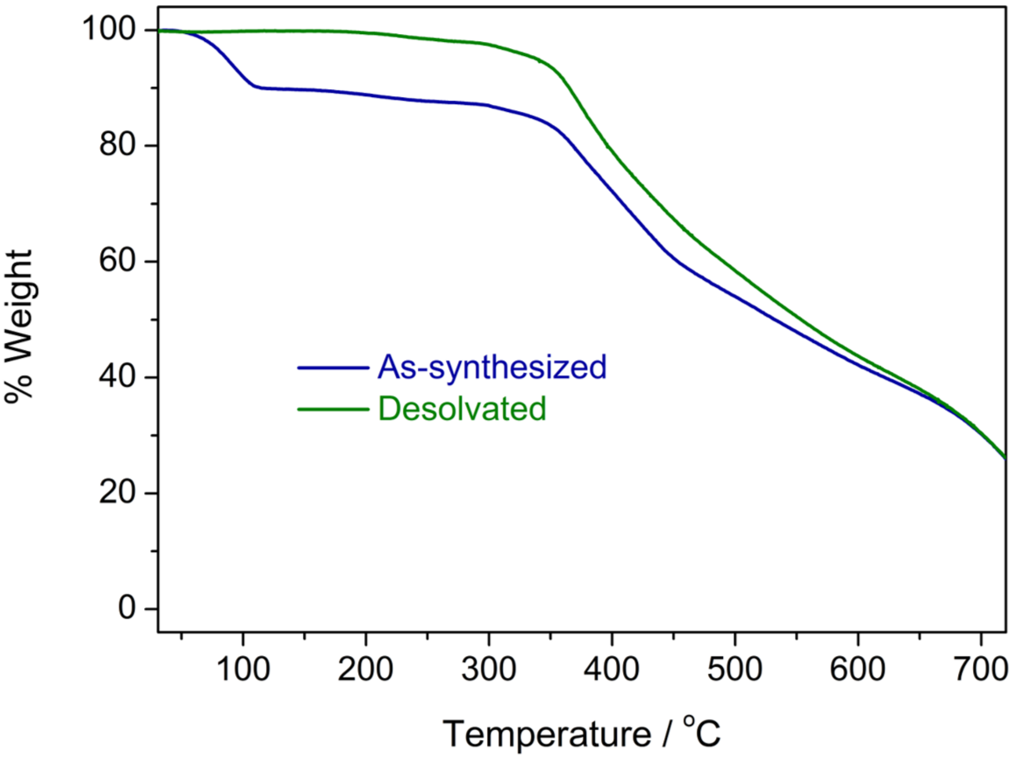

Figure S9: TGA profiles for compound iMOF-4C.

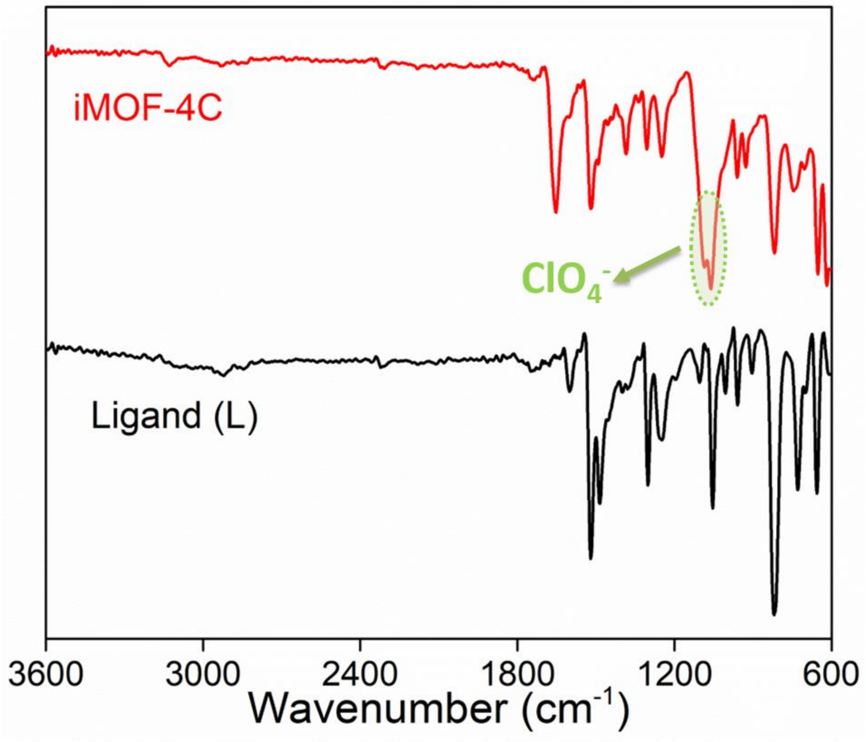

Figure S10: Infra-red (IR) spectroscopy of iMOF-4C showing the characteristic peaks of the framework anlong with the ClO_4^- anions.

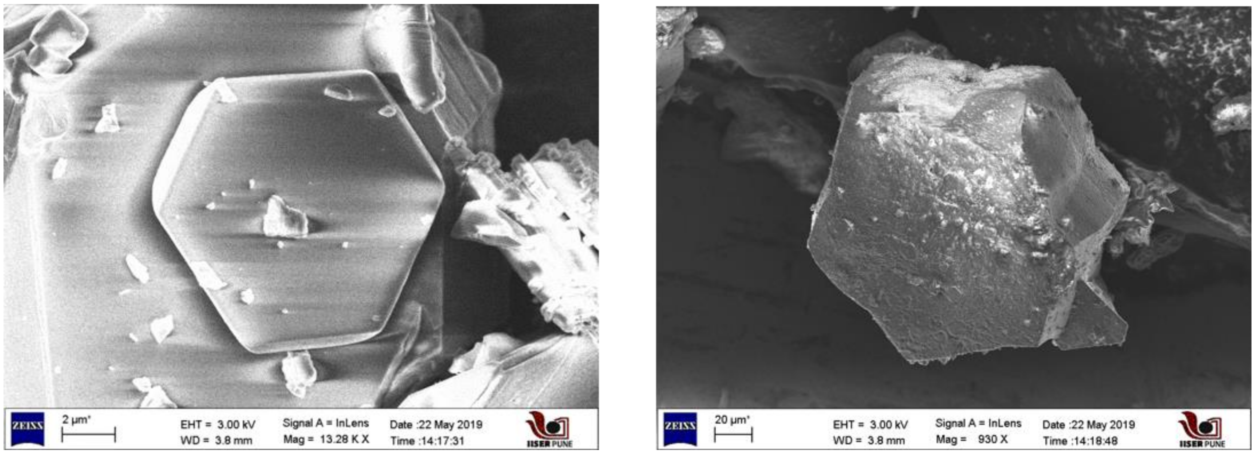

Figure S11: FESEM images of iMOF-4C.

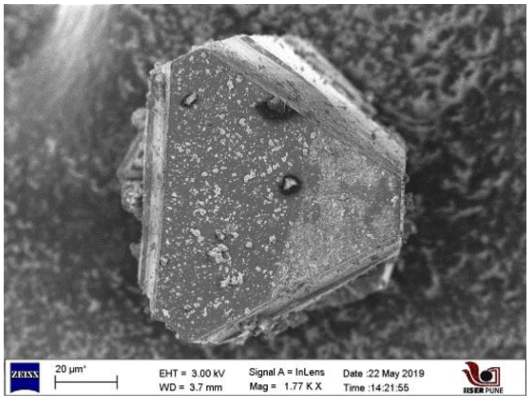

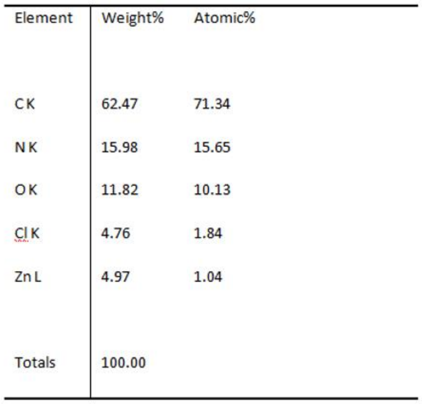

Element	Weight%	Atomic%
C K	62.47	71.34
N K	15.98	15.65
O K	11.82	10.13
Cl K	4.76	1.84
Zn L	4.97	1.04
Totals	100.00	

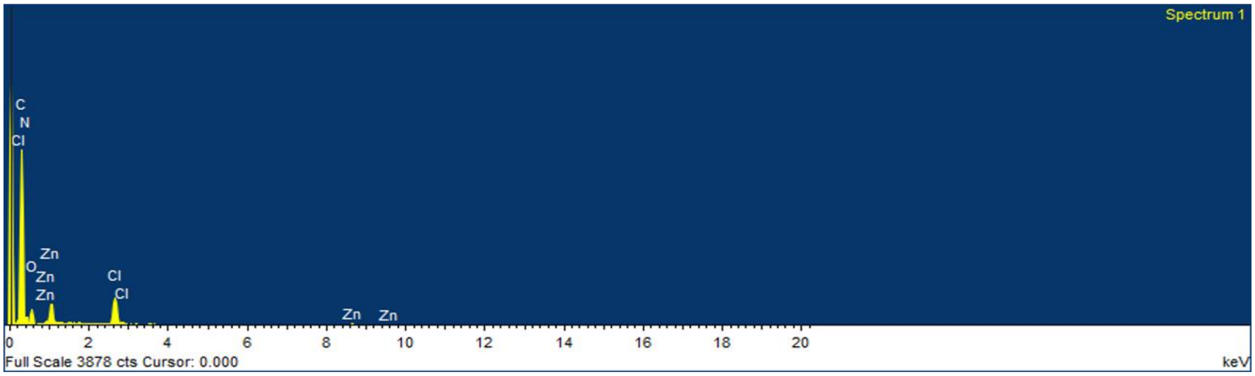

Figure S12: EDX analysis of iMOF-4C.

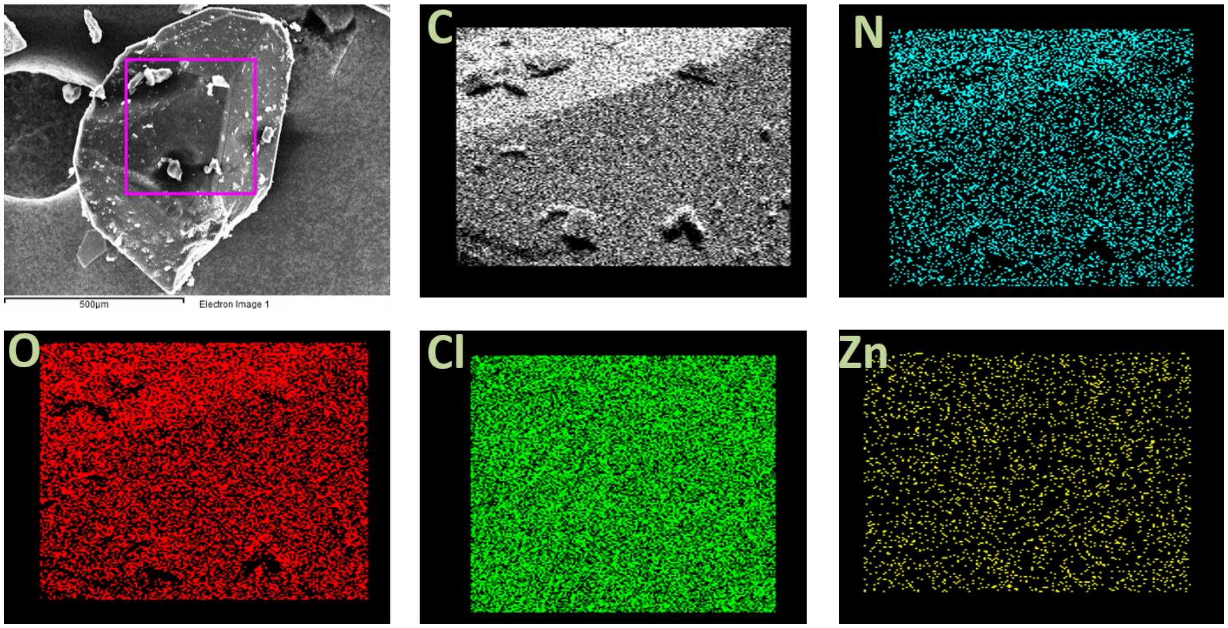

Figure S13: Elemental mapping of iMOF-4C.

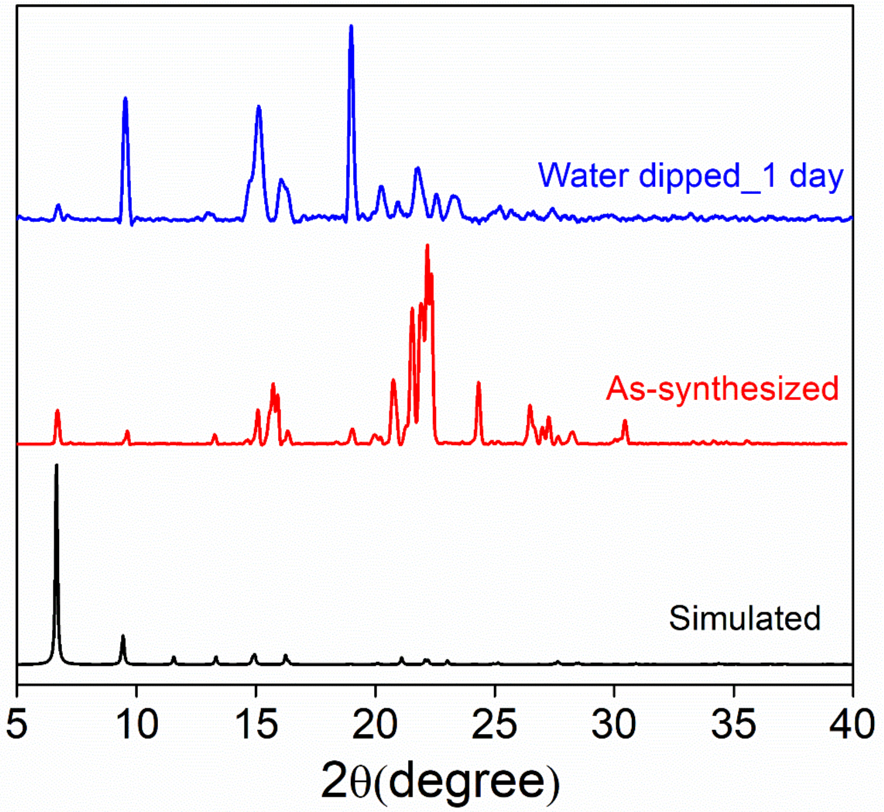

Figure S14: Powder X-ray diffraction patterns of iMOF-4C illustrating hydrolytic stability of the framework.

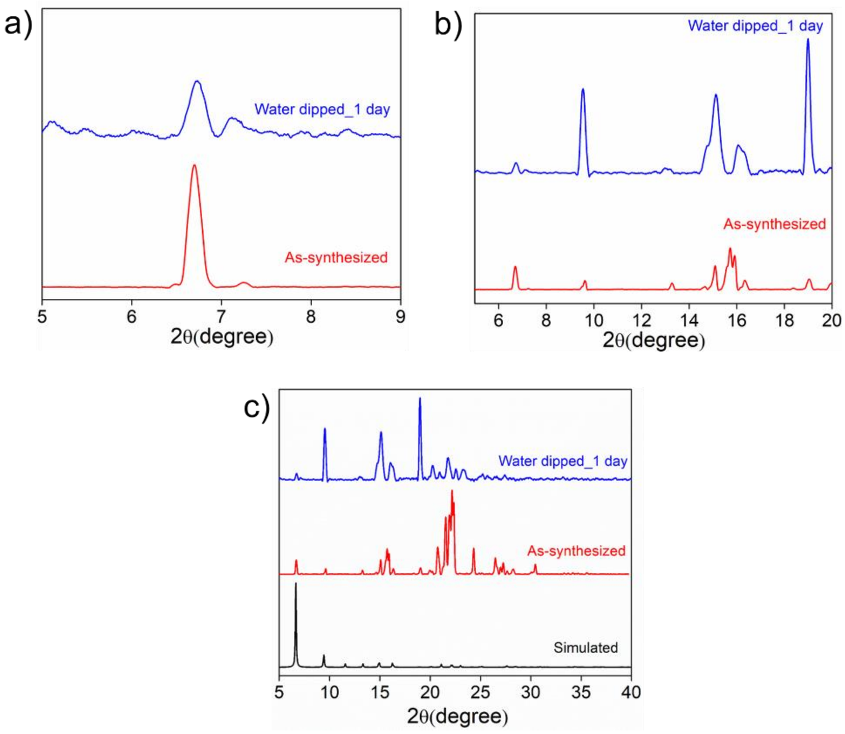

Figure S15: Powder X-ray diffraction patterns of iMOF-4C (a), (b) with zoomed view of the PXRD spectra. (c) PXRD spectra of pristine and water dipped phases.

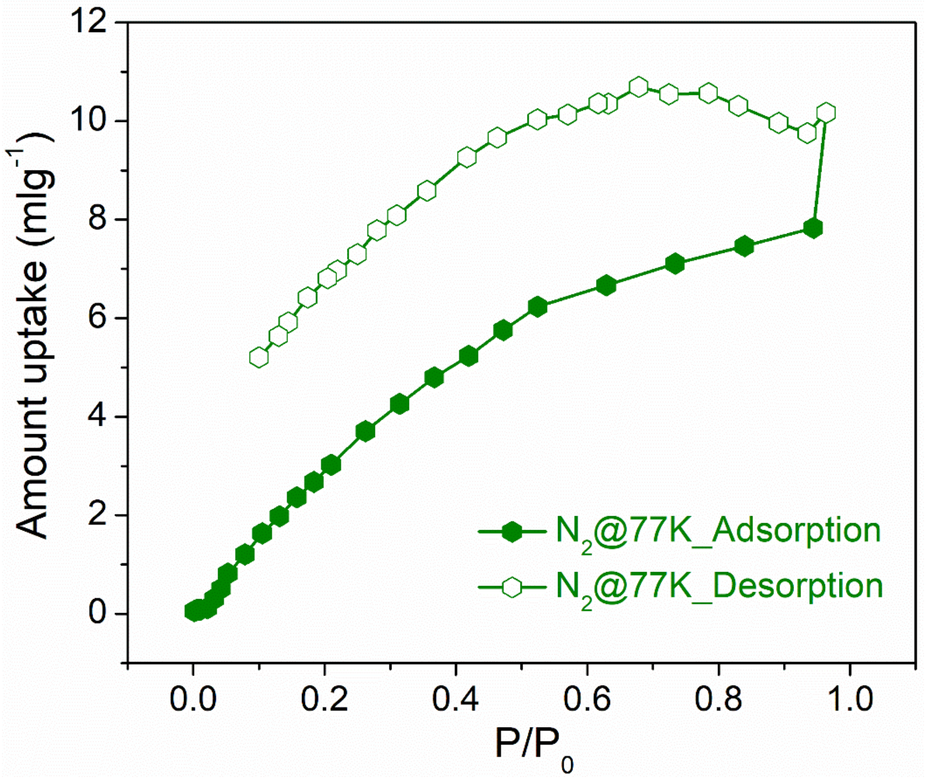

Figure S16: N_2 (77 K) adsorption isotherm of iMOF-4C.

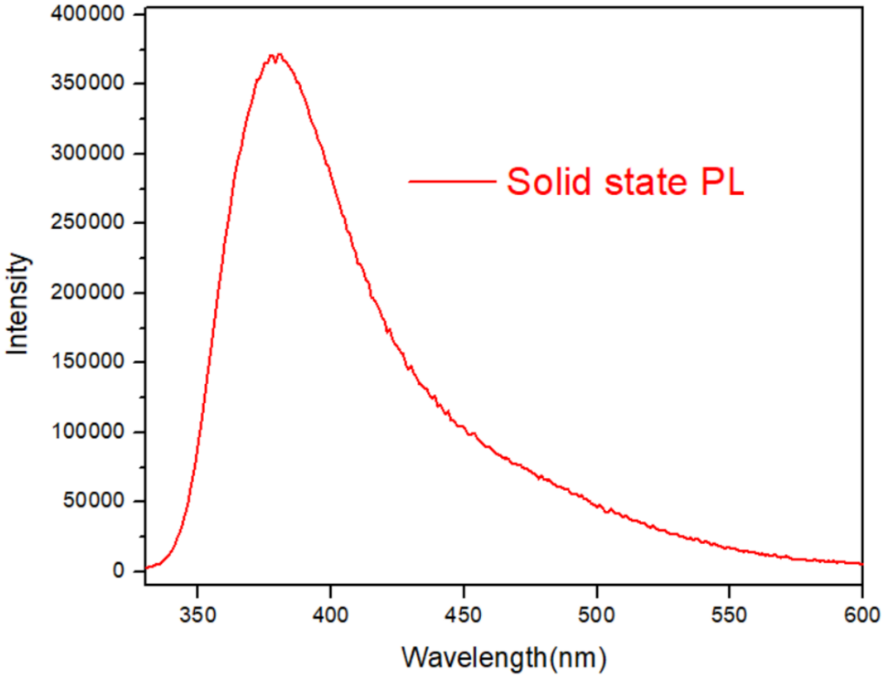

Figure S17: Solid state fluorescence spectra of iMOF-4C (λ_{ex}= 330nm).

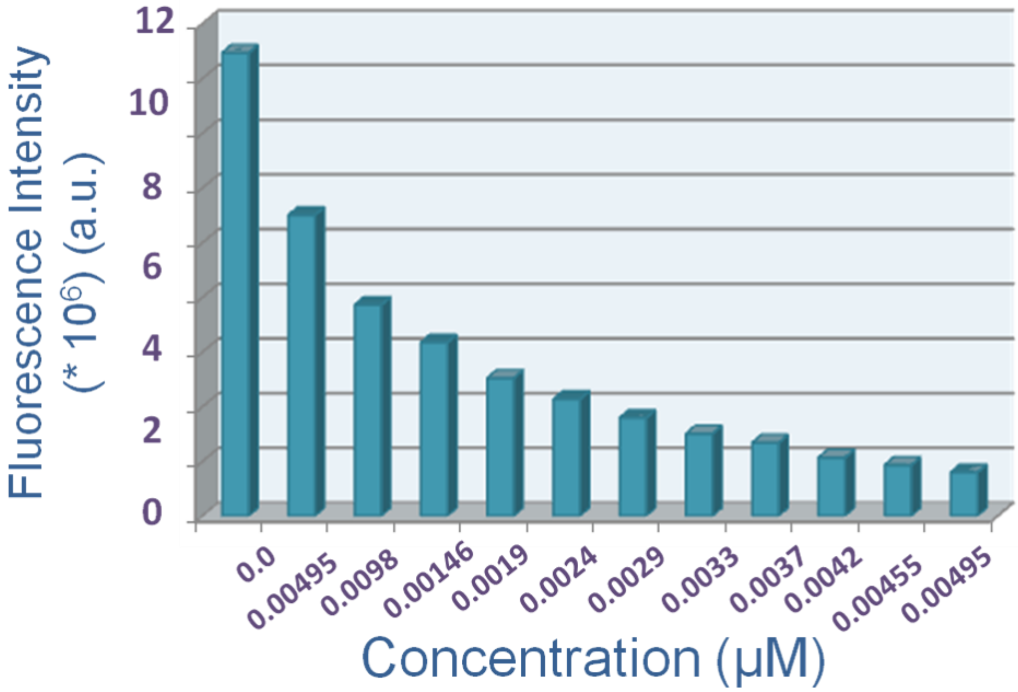

Figure S18: Change in the fluorescence intensity of iMOF-4C in water medium with increasing concentration of the CrO_4^{2-} anions at 378 nm.

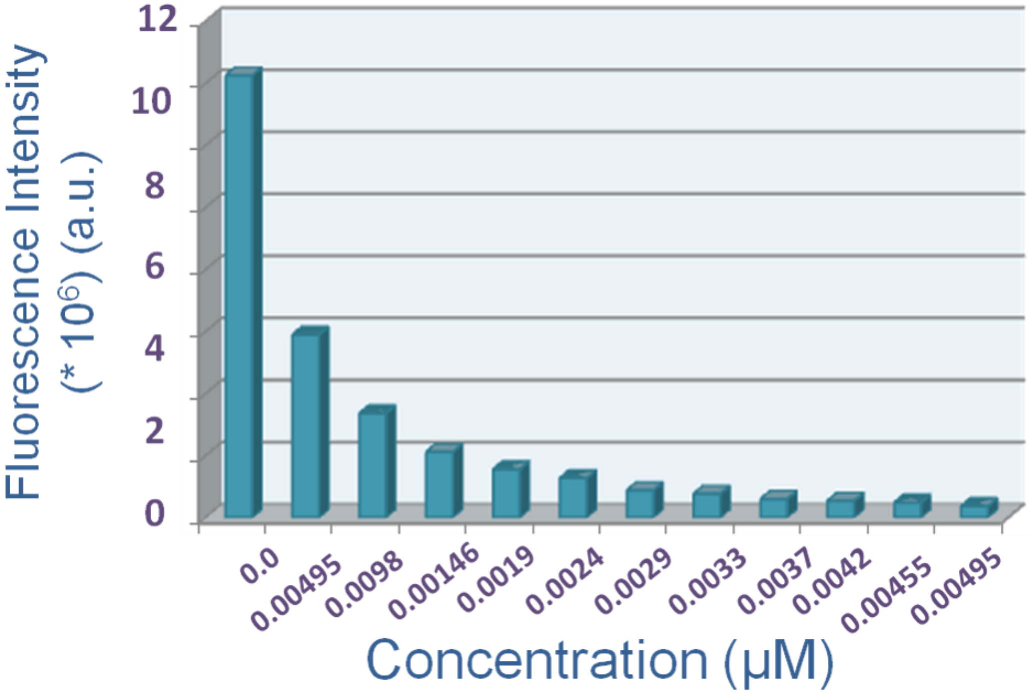

Figure S19: Change in the fluorescence intensity of iMOF-4C in water medium with increasing concentration of the $Cr_2O_7^{2-}$ anions at 378 nm.

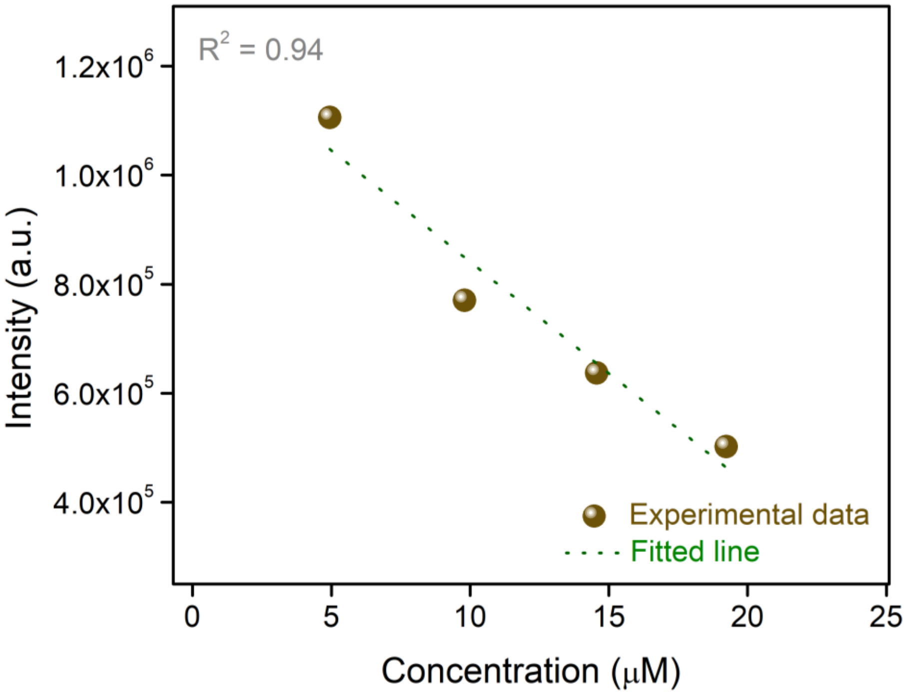

Figure S20: Linear region of fluorescence intensity of probe upon addition of CrO_4^{2-}; λ_{em}= 378 nm (upon excitation at 330 nm).

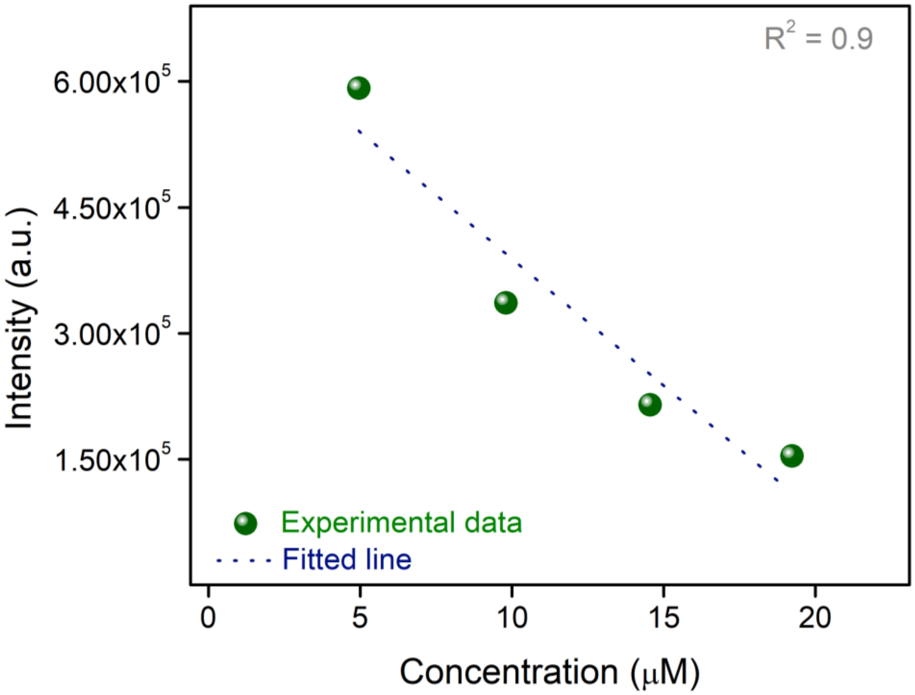

Figure S21: Linear region of fluorescence intensity of probe upon addition of $Cr_2O_7^{2-}$; λ_{em}= 378 nm (upon excitation at 330 nm).

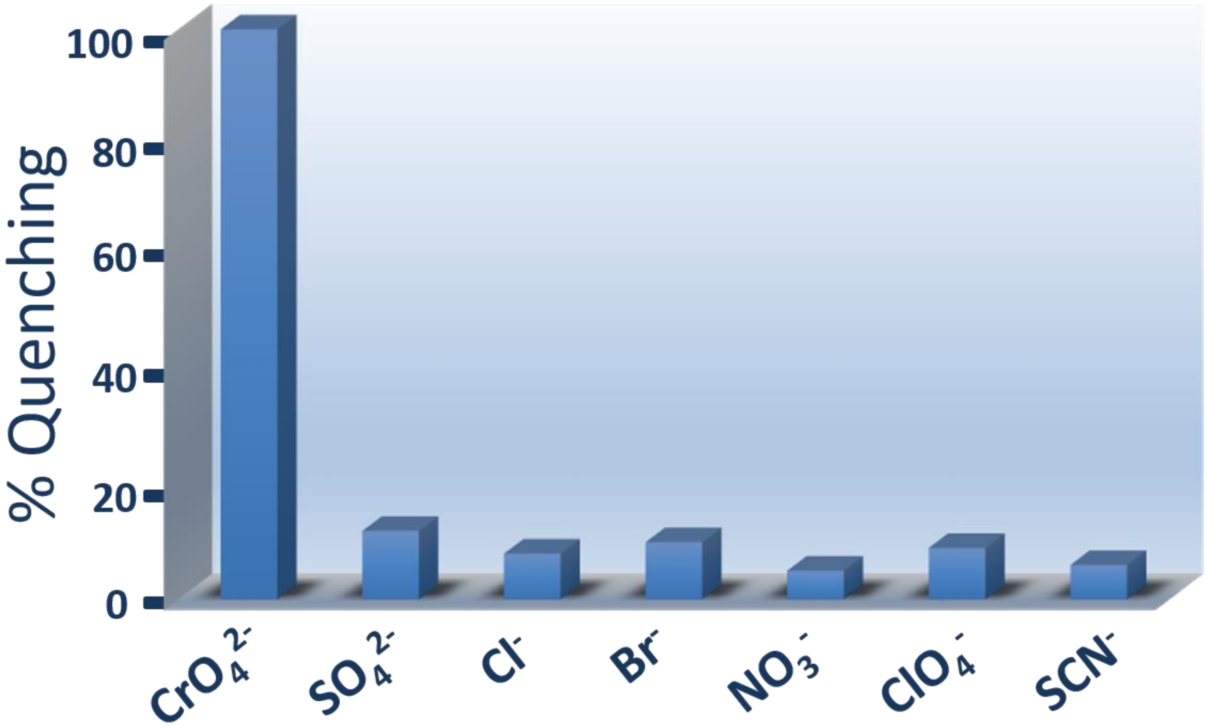

Figure S22: Percentage quenching of fluorescence emission of iMOF-4C toward CrO_4^{2-} and other competing anions.

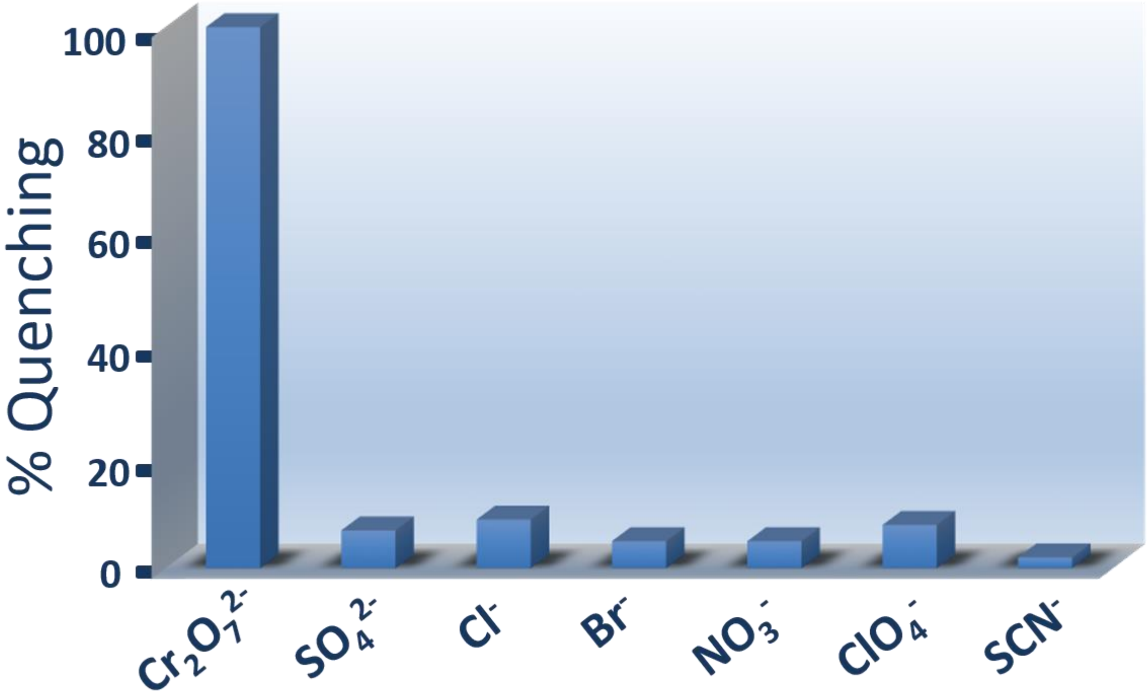

Figure S23: Percentage quenching of fluorescence emission of iMOF-4C toward $Cr_2O_7^{2-}$ and other competing anions.

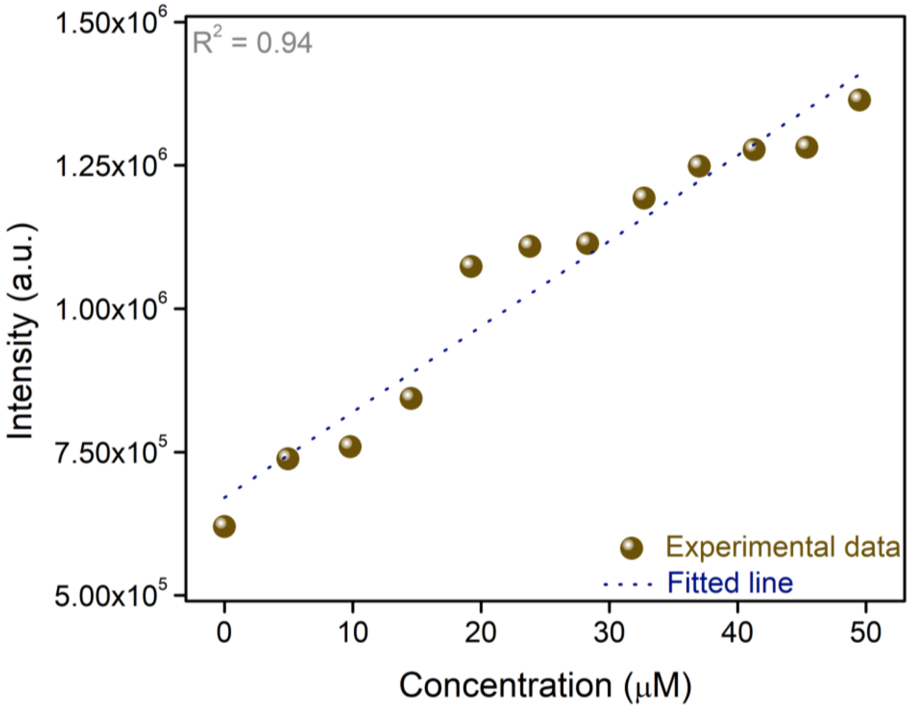

Figure S24: Linear region of fluorescence intensity of probe upon addition of $HAsO_4^{2-}$; λ_{em}= 378 nm (upon excitation at 330 nm).

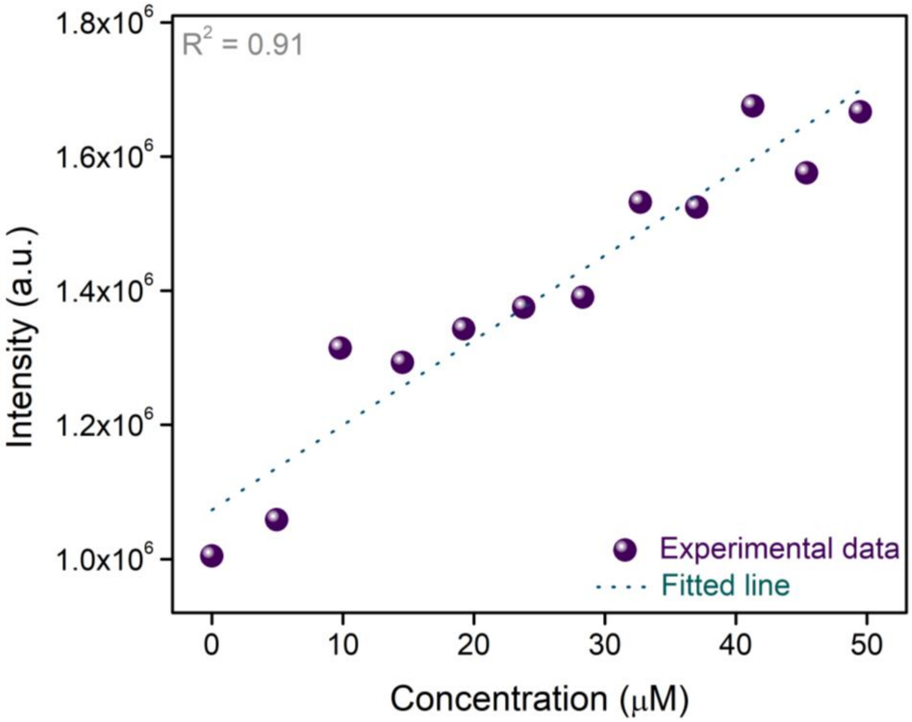

Figure S25: Linear region of fluorescence intensity of probe upon addition of $HAsO_3^{2-}$; λ_{em}= 378 nm (upon excitation at 330 nm).

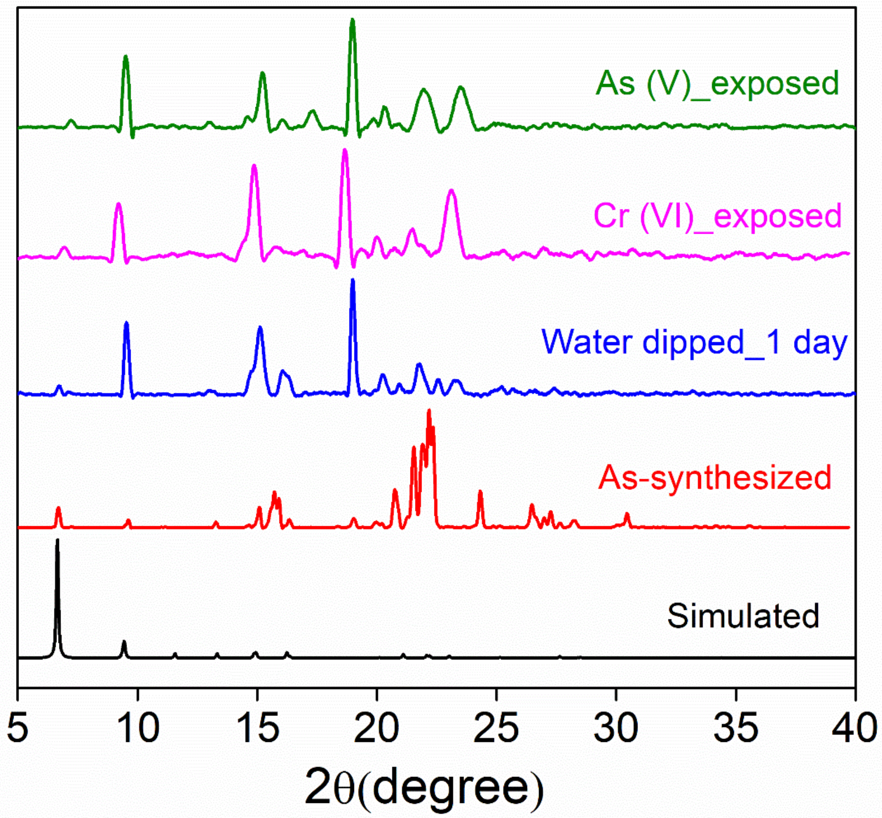

Figure S26: Powder X-ray diffraction patterns of iMOF-4C.

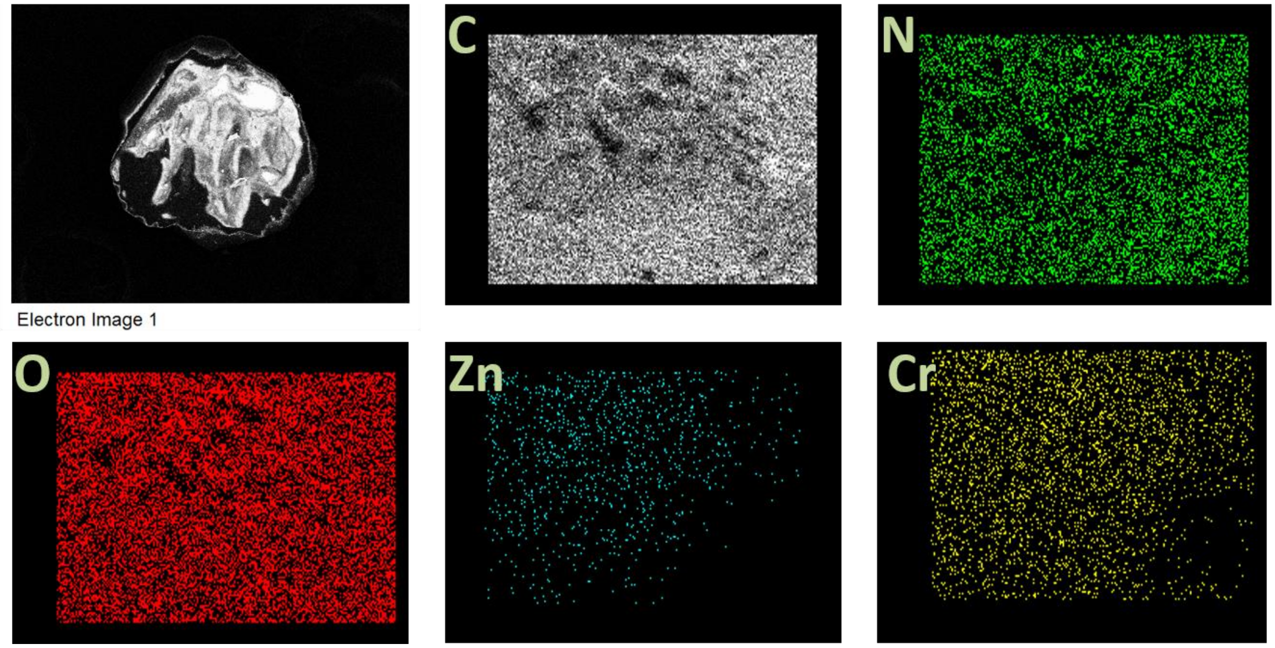

Figure S27: Elemental mapping of iMOF-4C@CrO_4^{2-}.

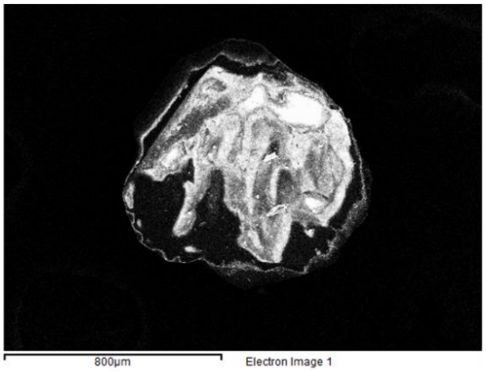

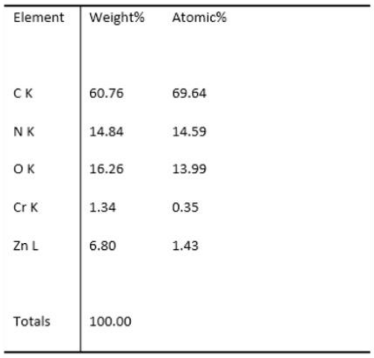

Element	Weight%	Atomic%
C K	60.76	69.64
N K	14.84	14.59
O K	16.26	13.99
Cr K	1.34	0.35
Zn L	6.80	1.43
Totals	100.00	

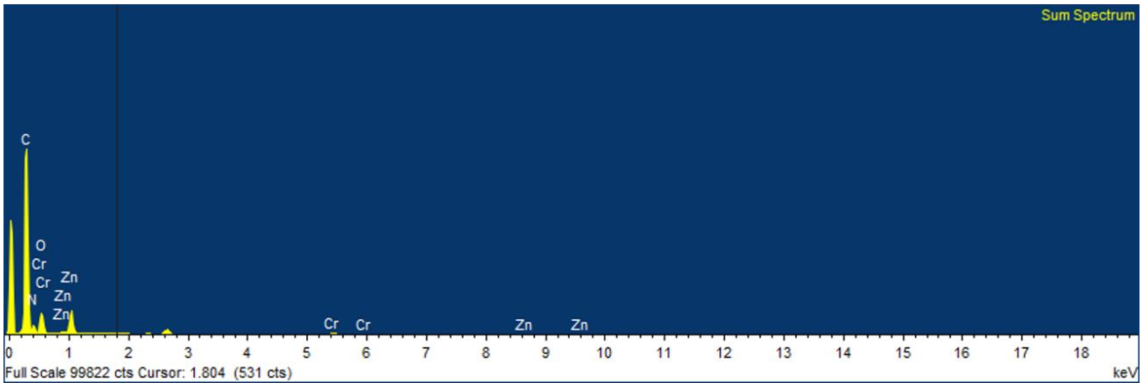

Figure S28: EDX analysis of iMOF-4C.@CrO42-.

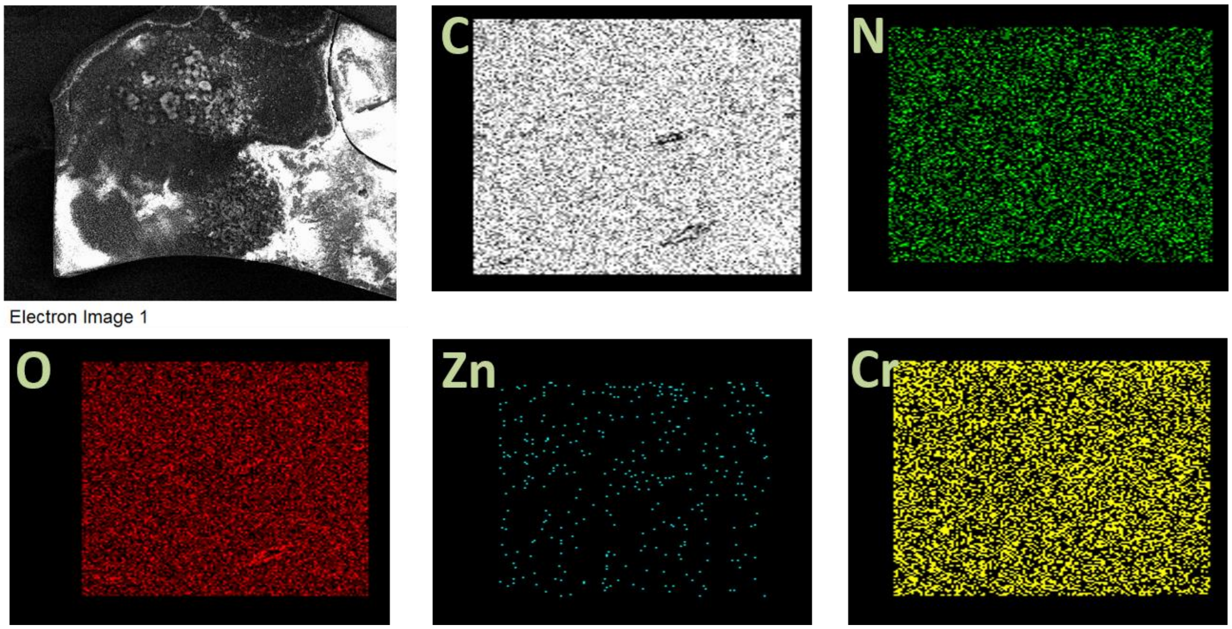

Figure S29: Elemental mapping of iMOF-4C@$Cr_2O_7^{2-}$.

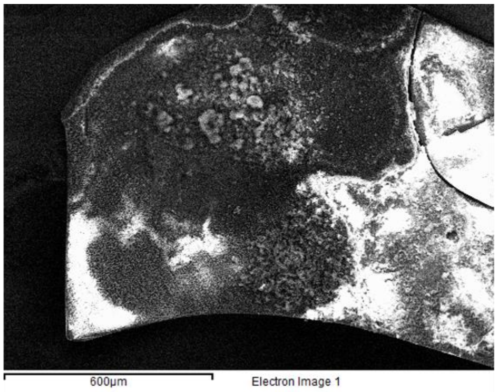

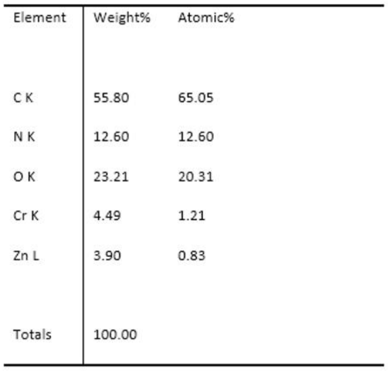

Element	Weight%	Atomic%
C K	55.80	65.05
N K	12.60	12.60
O K	23.21	20.31
Cr K	4.49	1.21
Zn L	3.90	0.83
Totals	100.00	

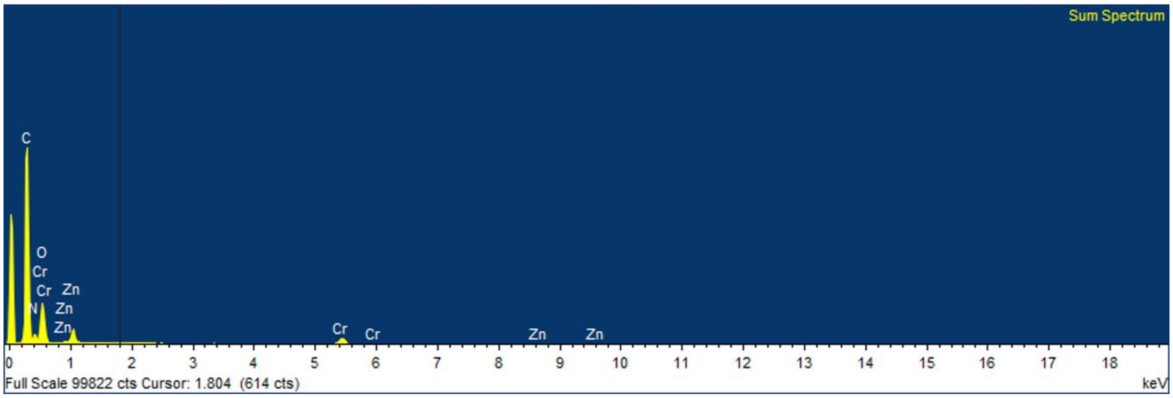

Figure S30: EDX analysis of iMOF-4C.@$Cr_2O_7^{2-}$.

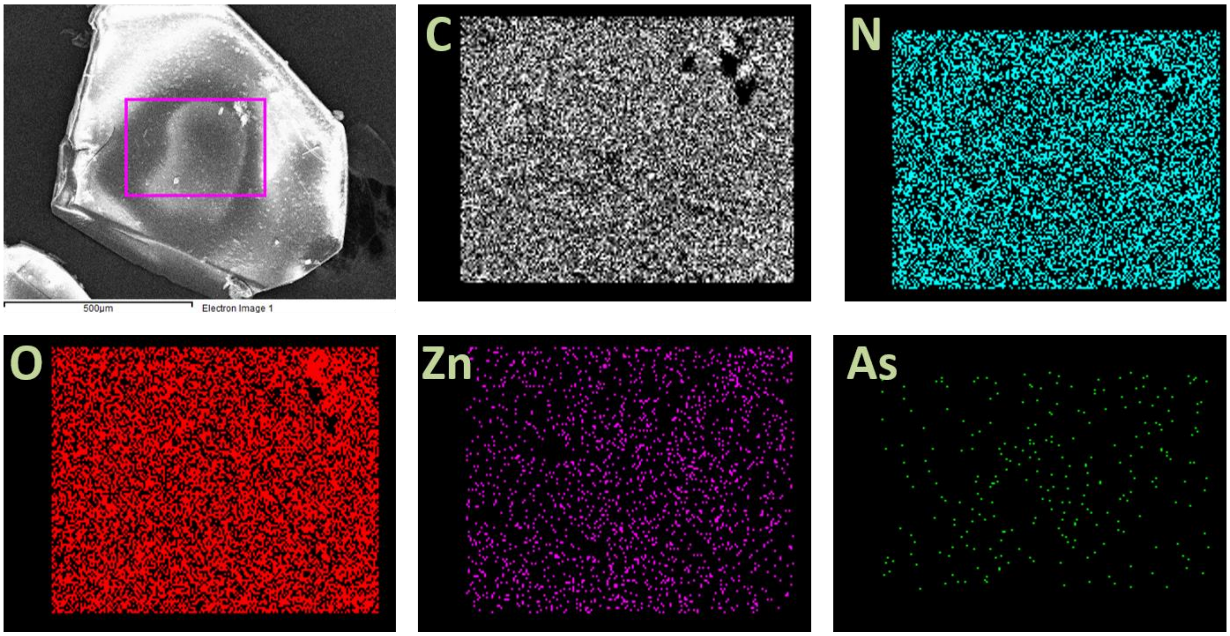

Figure S31: Elemental mapping of iMOF-4C@$HAsO_4^{2-}$.

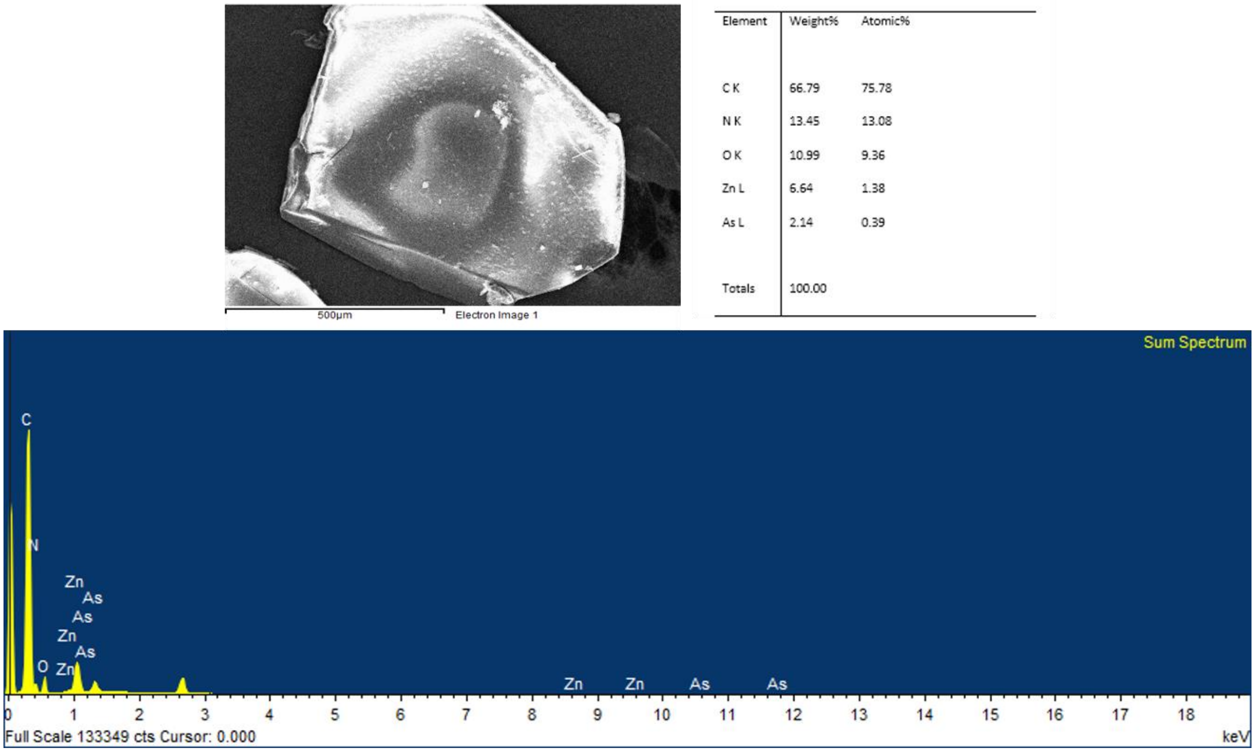

Element	Weight%	Atomic%
C K	66.79	75.78
N K	13.45	13.08
O K	10.99	9.36
Zn L	6.64	1.38
As L	2.14	0.39
Totals	100.00	

Figure S32: EDX analysis of iMOF-4C@$HAsO_4^{2-}$.

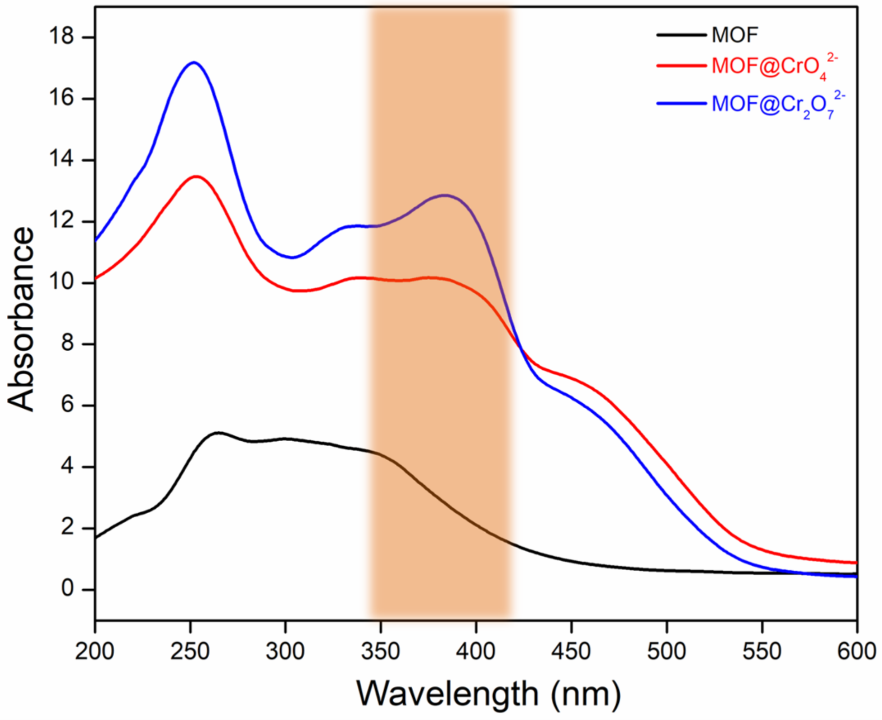

Figure S33: solid state UV-vis spectra of iMOF-4C.

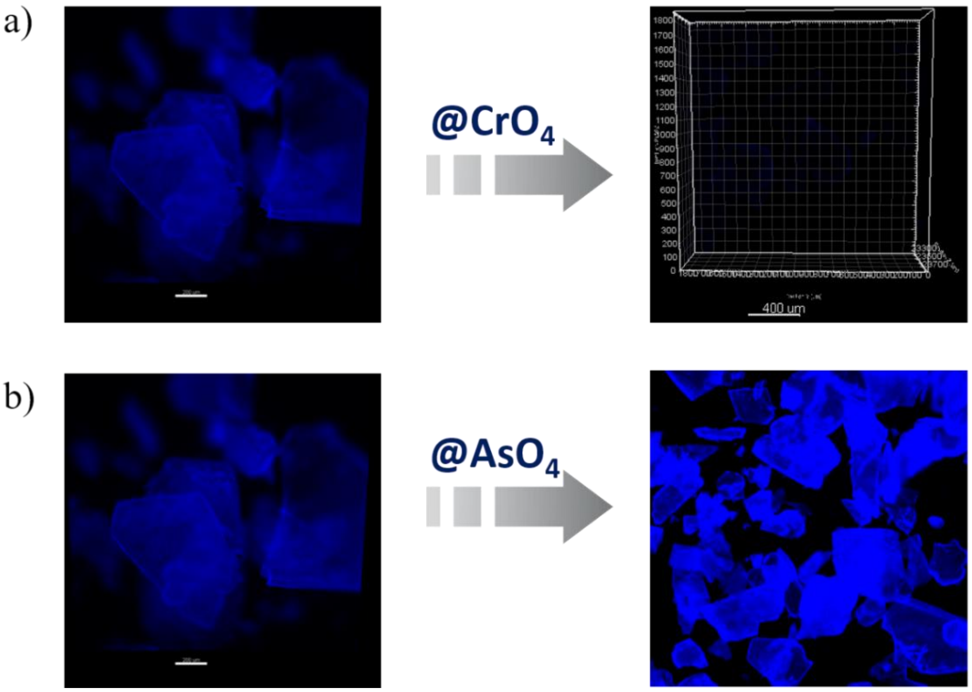

Figure S34: Change in confocal fluorescence imaging of iMOF-4C upon addition of (a) CrO_4^{2-}, (b) $HAsO_4^{2-}$.

Anion exchange studies

The cationic nature of iMOF-4C prompted us to check its potential toward sequestration of these oxo-anions. For this, we have carried out an *in-situ* titration under UV−vis spectroscopy with aqueous solution of CrO_4^{2-} anions (2 mL, 0.5 mM) and 1 mg of iMOF-4C via monitoring absorption maxima (λmax) at 372 nm (Figure S33). A gradual decremental trend in absorption profile was observed with increasing time intervals affirmed the capture of CrO_4^{2-} anions by iMOF-4C. The anion trapping process was found to be kinetically rapid which is further advocated from the % removal vs time plot (Figure S34-S35). Additionally, the anion capture process was found to follow the pseudo second order kinetics (Figure S36).

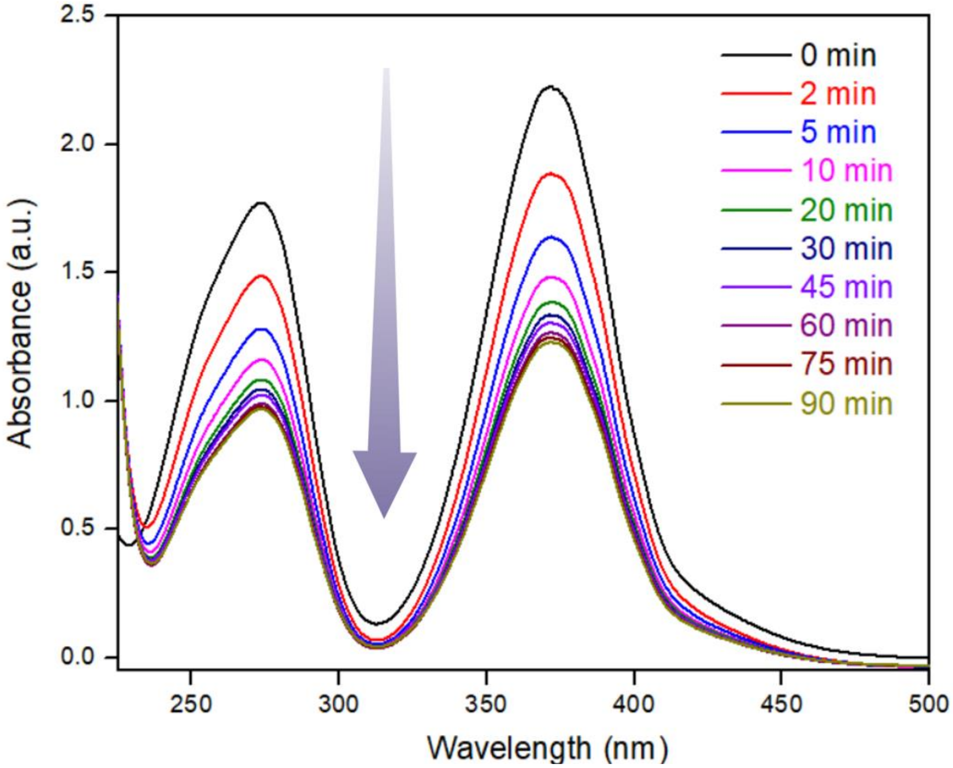

Figure S35: UV−vis spectra in the presence of iMOF-4C for CrO_4^{2-}.

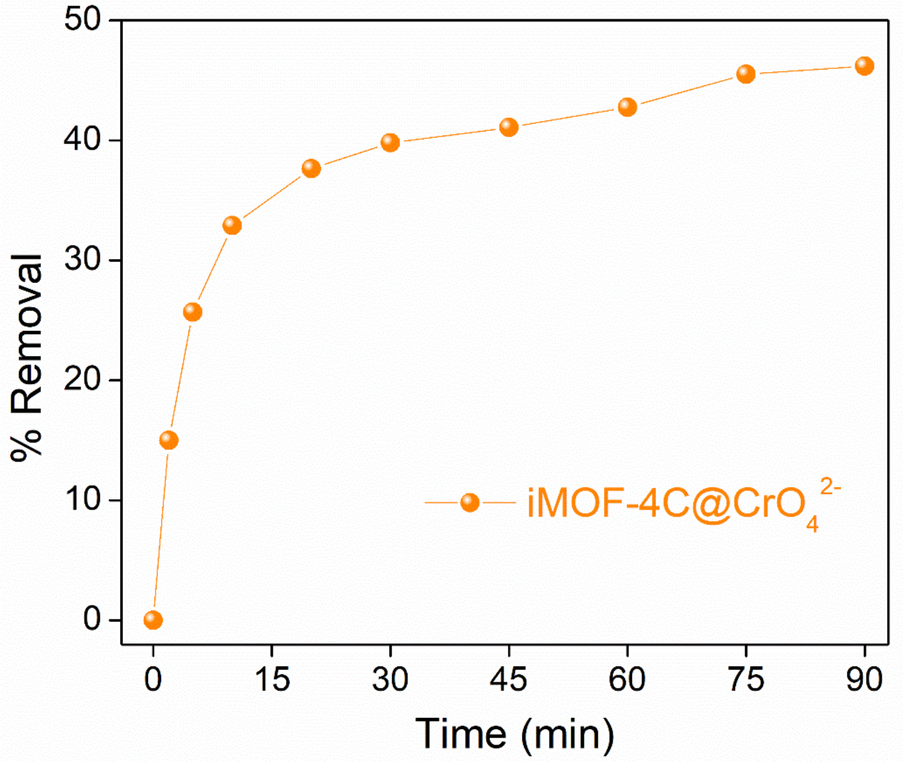

Figure S36: Removal (in %) of CrO_4^{2-} with iMOF-4C at different time intervals.

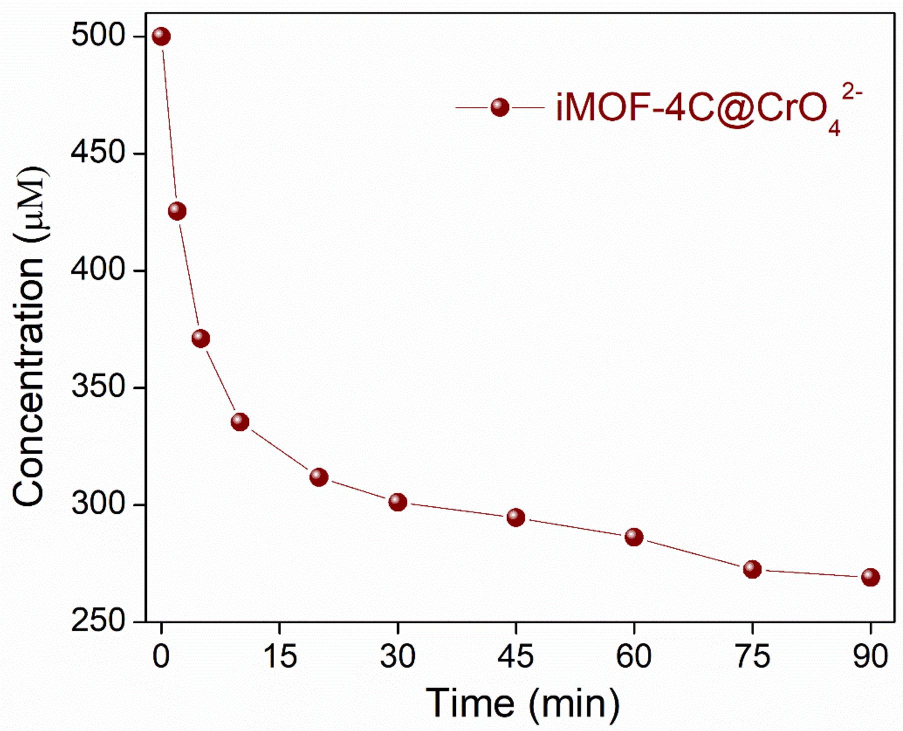

Figure S37: Decrease in concentration of CrO_4^{2-} with iMOF-4C at different time intervals.

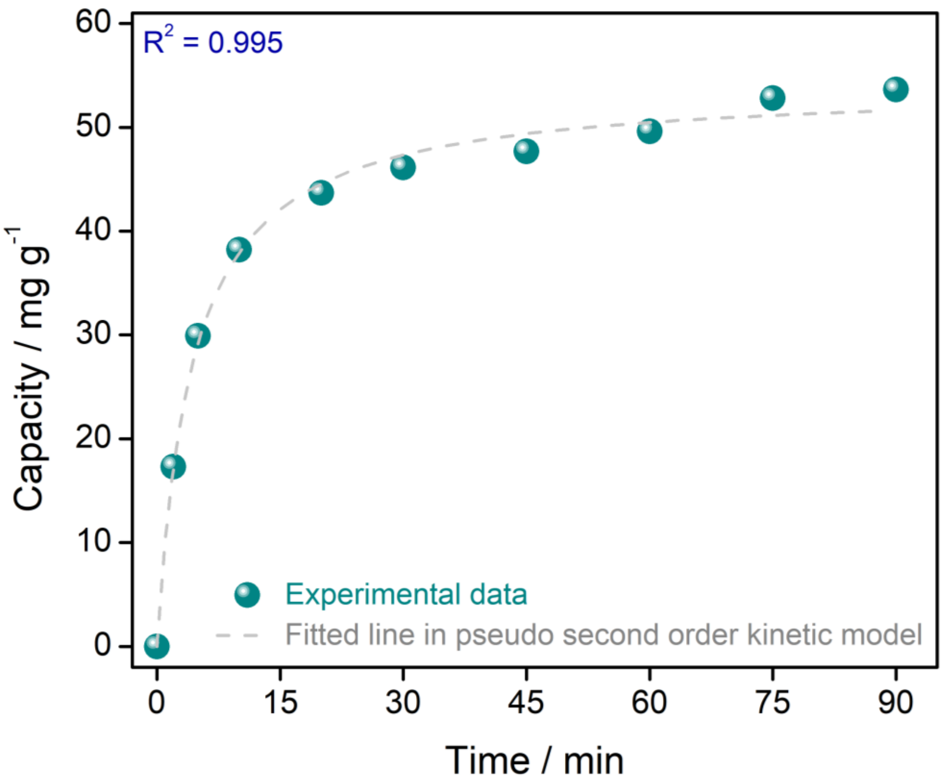

Figure S38: Kinetic study of CrO_4^{2-} ion capture with iMOF-4C.

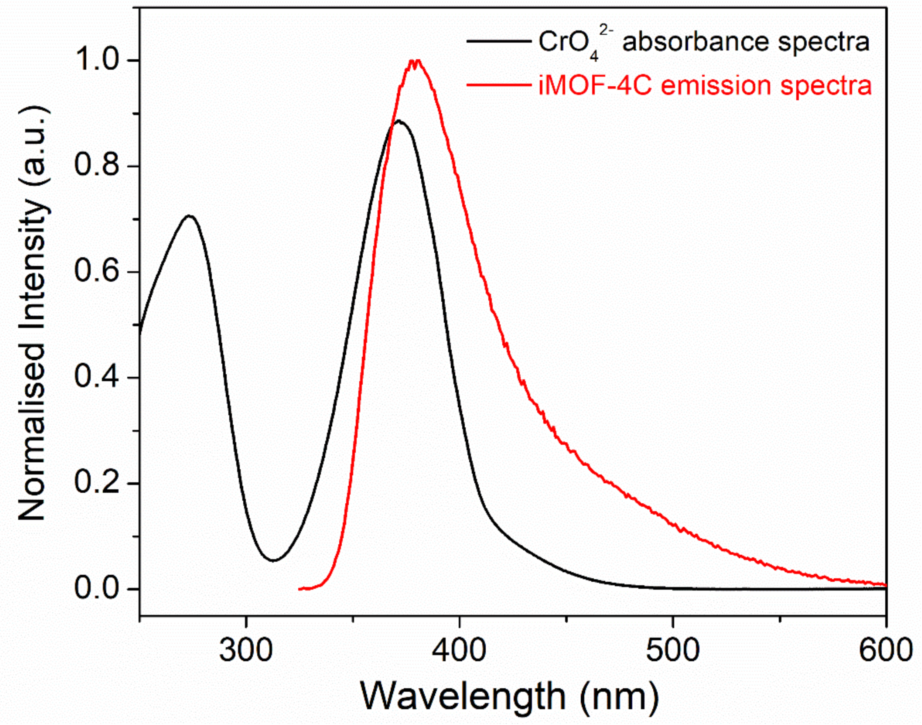

Figure S39: Absorbance and emission spectra of CrO_4^{2-} and iMOF-4C respectively.

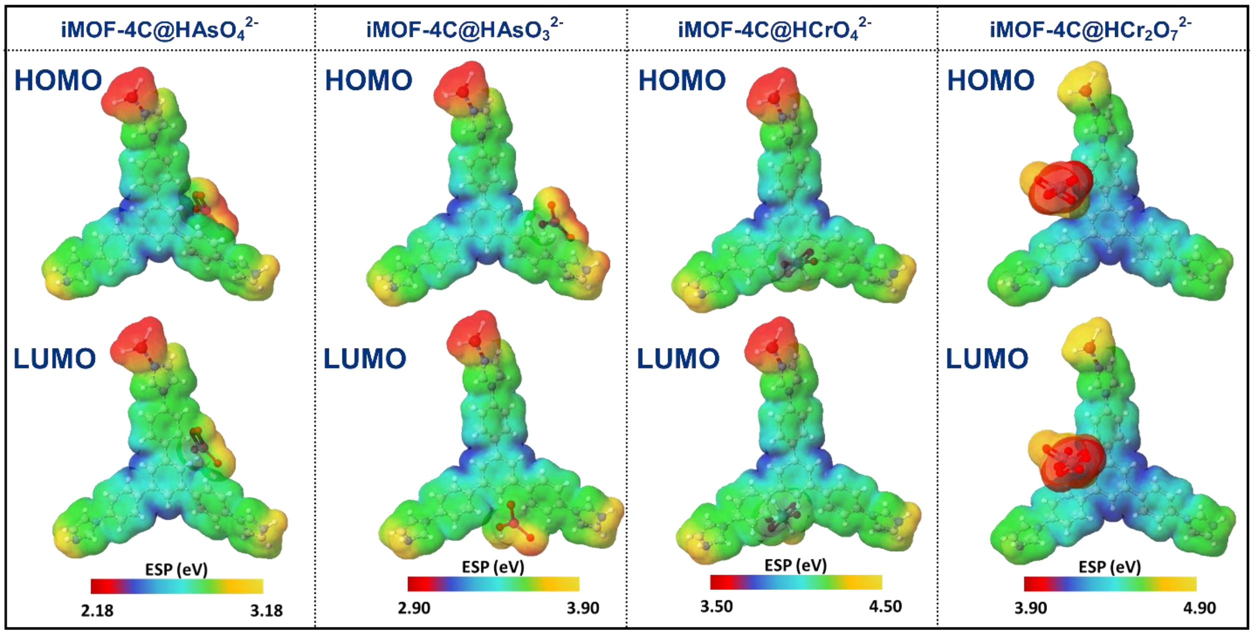

Figure S40: Electron density map of HOMO and LUMO energy state of iMOF-4C showing the change in electronic properties of the framework in presence of different oxo-anions.

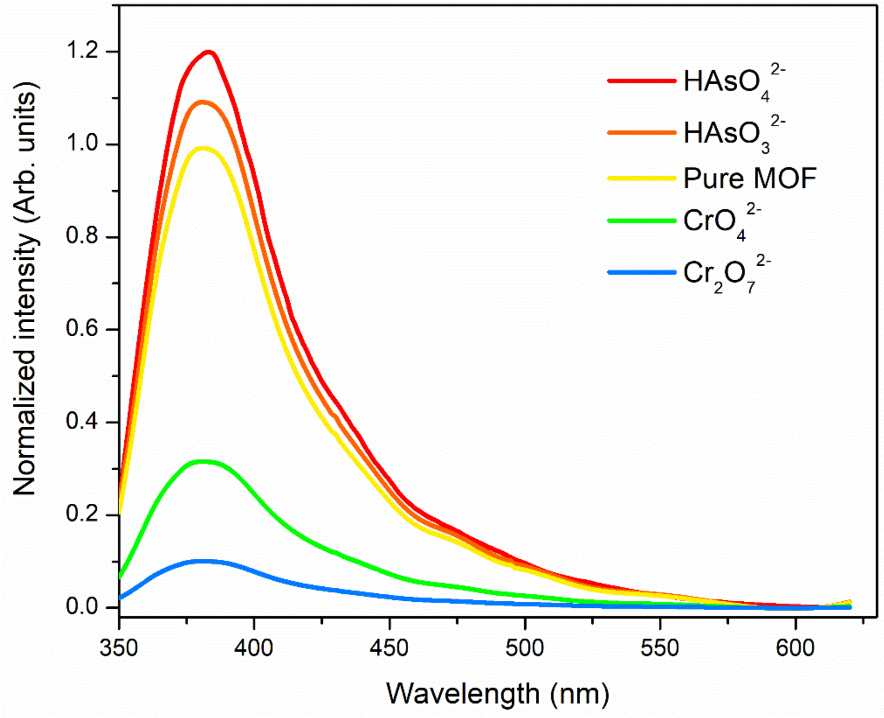

Figure S41: Theoretically predicted emission profiles for iMO-4C and change in emission upon interacting with different anions based on DFT calculations on single unit.

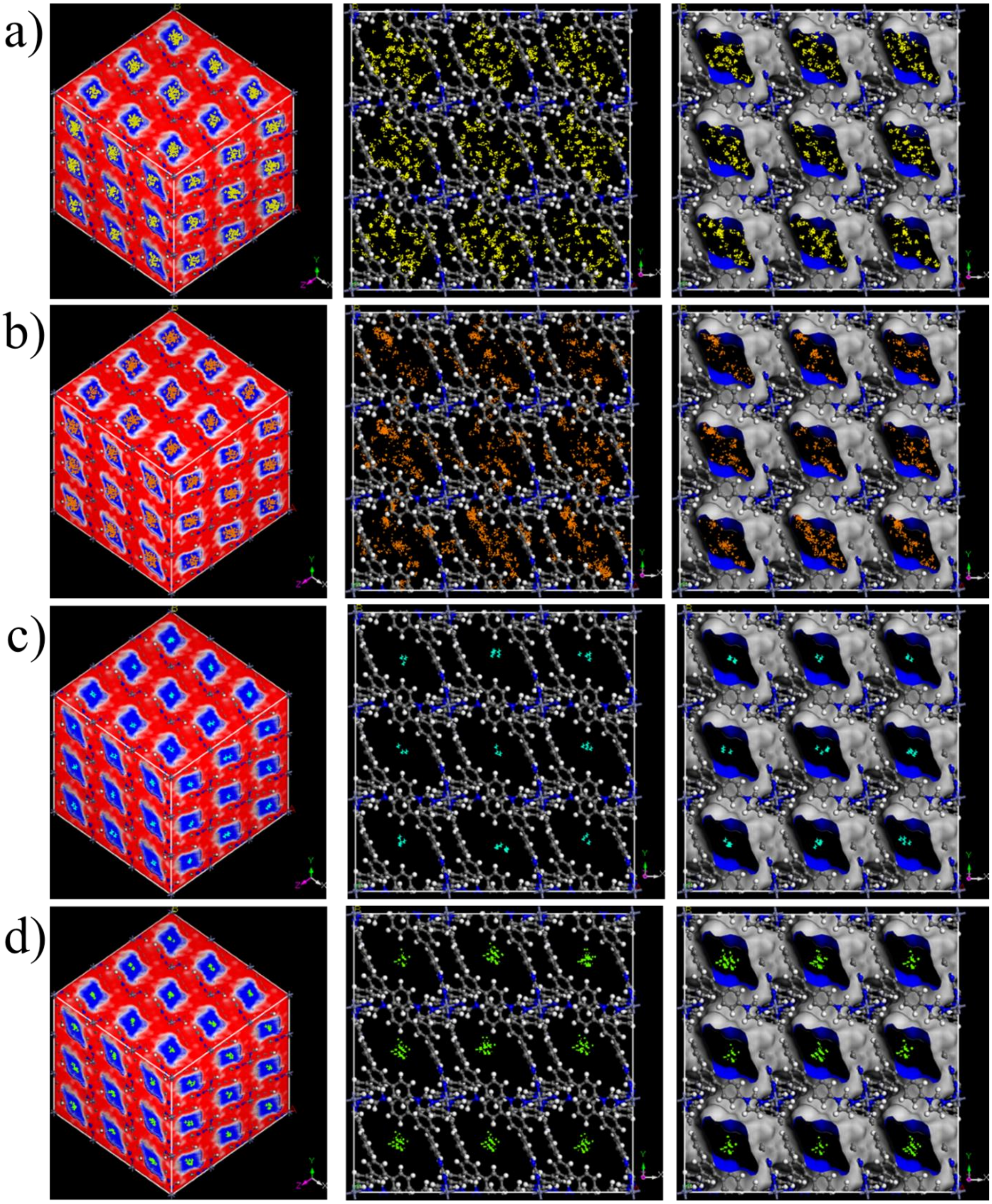

Figure S42: Electron density map for (a) $Cr_2O_7^{2-}$, (b) CrO_4^{2-}, (c) $HAsO_4^{2-}$ and (d) $HAsO_3^{2-}$.

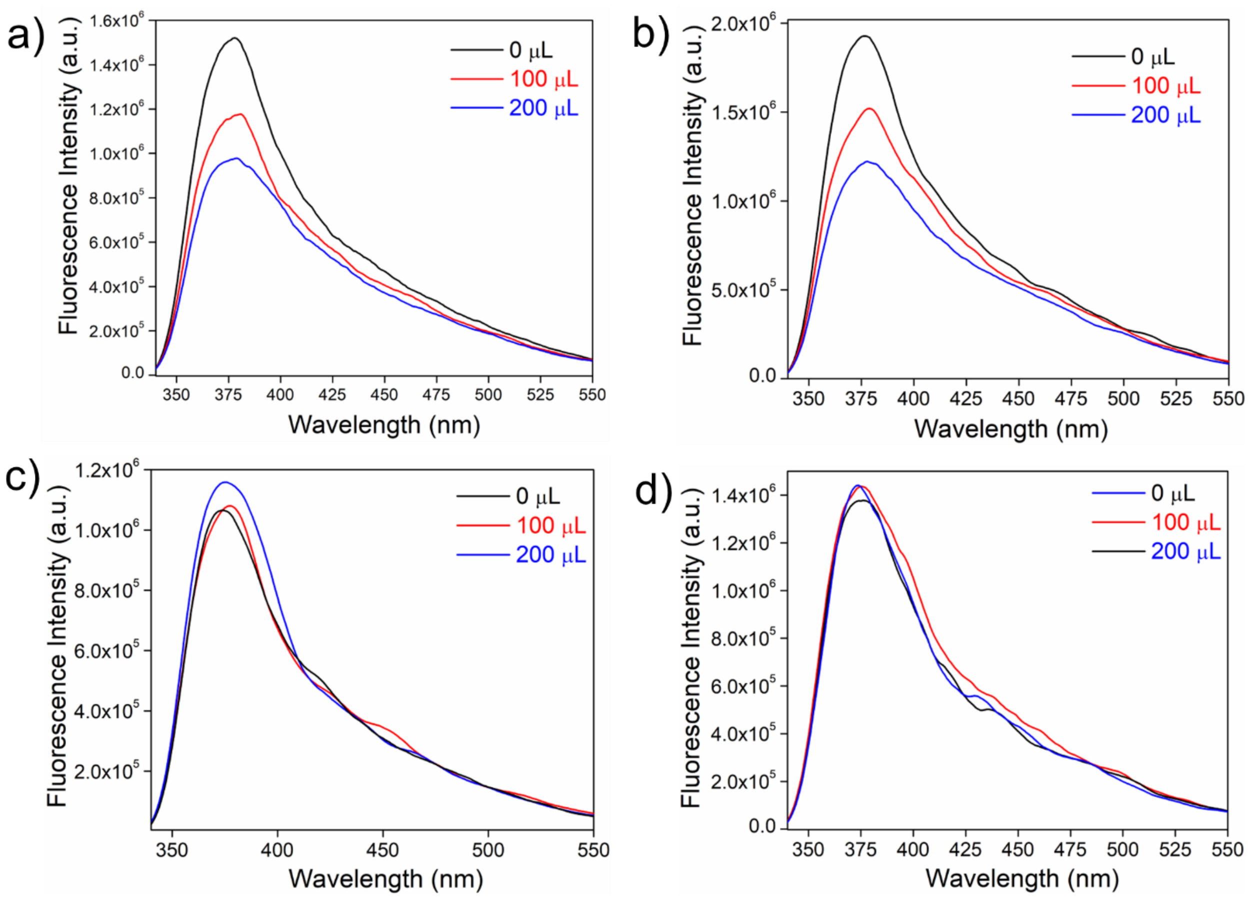

Figure S43: Fluorescence responses of the only ligand (L) in presence (a) CrO_4^{2-}, (b) $Cr_2O_7^{2-}$, (c) $HAsO_4^{2-}$ and (d) $HAsO_3^{2-}$.

Table S1: A comparison table of Sensing performance in MOF based materials for $CrO_4{}^{2-}$ and $Cr_2O_7{}^{2-}$ with some well-studied examples in the literature.

MOF	Analyte	K_{sv} (M^{-1})	LOD (mol/L)	Medium	Mode of Sensing	Reference
Comparison with other MOFs based CrO_4^{2-} sensors						
iMOF-4C	**$CrO_4{}^{2-}$**	**1.31×10^5**	**3.06×10^{-6}**	**Water**	**Luminescence Quenching**	**This Work**
$[Zn_3(L)(OH)(H_2O)_5]\cdot NMP\cdot 2H_2O$	$CrO_4{}^{2-}$	1.3×10^4	4.29×10^{-4}	Water	Luminescence Quenching	9
$[Cd(L)_2(H_2O)_2]$	$CrO_4{}^{2-}$	1.1×10^4	1.75×10^{-4}	Water	Luminescence Quenching	10
$[Zn_2(TPOM)(NDC)_2]\cdot 3.5H_2O$	$CrO_4{}^{2-}$	7.81×10^3	2.5×10^{-6}	Water	Luminescence Quenching	11
$[Tb(L)(HCOO)(H_2O)]$	CrO_4^{2-}	1.3×10^3	1.8×10^{-6}	Water	Luminescence Quenching	12
$[Eu(L)(HCOO)(H_2O)]n$	$CrO_4{}^{2-}$	1.5×10^3	1.2×10^{-6}	Water	Luminescence Quenching	13
$[Zn_2(TPOM)(NH_2–BDC)_2]\cdot 4H_2O$	$CrO_4{}^{2-}$	$4.45X10^3$	4.8×10^{-6}	DMF	Luminescence Quenching	14
$[Zn(btz)]_n$	$CrO_4{}^{2-}$	$3.19X10^3$	1×10^{-5}	Water	Luminescence Quenching	15
$[Zn_2(ttz)H_2O]_n$	$CrO_4{}^{2-}$	$2.35X10^3$	2×10^{-5}	Water	Luminescence Quenching	15
$[Zn(L)(H_2O)]\cdot H_2O$	$CrO_4{}^{2-}$	1.02×10^4	4.8×10^{-6}	Water	Luminescence Quenching	16
$[Eu(L)(H_2O)(DMA)]$	$CrO_4{}^{2-}$	5.33×10^4	7.30×10^{-6}	Water	Luminescence Quenching	17
Comparison with other MOFs based $Cr_2O_7^{2-}$ sensors						
iMOF-4C	**$Cr_2O_7{}^{2-}$**	**4.85×10^5**	**4.15×10^{-6}**	**Water**	**Luminescence Quenching**	**This Work**
$[Zn_3(L)(OH)(H_2O)_5]\cdot NMP\cdot 2H_2O$	$Cr_2O_7{}^{2-}$	6.6×10^4	6.05×10^{-5}	Water	Luminescence Quenching	9
$[Cd(L)_2(H_2O)_2]$	$Cr_2O_7{}^{2-}$	5.1×10^4	3.41×10^{-5}	Water	Luminescence Quenching	10
$[Tb(TBOT)(H_2O)](H_2O)_4(DMF)(NMP)_{0.5}$	$Cr_2O_7{}^{2-}$	1.37×10^4	1.4×10^{-4}	Water	Luminescence Quenching	18
$[Zn(L)(H_2O)]\cdot H_2O$	$Cr_2O_7{}^{2-}$	2.07×10^4	3.53×10^{-6}	Water	Luminescence Quenching	16
$[Zn_2(TPOM)(NH_2–BDC)_2]\cdot 4H_2O$	$Cr_2O_7{}^{2-}$	$7.59X10^3$	3.9×10^{-6}	DMF	Luminescence Quenching	14
Eu_4L_3	$Cr_2O_7{}^{2-}$	$1.52X10^3$	10×10^{-6}	DMF	Luminescence Quenching	19

$[Tb(TATAB)(H_2O)_2]\cdot NMP$	$Cr_2O_7\ ^{2-}$	$1.11X10^4$	1×10^{-6}	Water	Luminescence Quenching	20
Eu^{3+}@MIL-121	$Cr_2O_7\ ^{2-}$	$4.34X10^3$	0.05×10^{-6}	Water	Luminescence Quenching	21
$[Zn(btz)]_n$	$Cr_2O_7\ ^{2-}$	$4.23X10^3$	2×10^{-6}	Water	Luminescence Quenching	15
$[Zn_2(ttz)H_2O]_n$	$Cr_2O_7\ ^{2-}$	$2.19X10^3$	2×10^{-5}	Water	Luminescence Quenching	15

Table 2. Crystal data and structure refinement for iMOF-4C.

Identification code	iMOF-4C	
CCDC Number	2073931	
Empirical formula	C66 H48 N12 Zn	
Formula weight	1074.53	
Temperature	296(2) K	
Wavelength	0.71073 Å	
Crystal system	Trigonal	
Space group	R -3 :H	
Unit cell dimensions	a = 18.7016(16) Å	α= 90°.
	b = 18.7016(16) Å	β= 90°.
	c = 23.159(2) Å	γ = 120°.
Volume	7014.7(14) Å^3	
Z	3	
Density (calculated)	0.763 Mg/m^3	
Absorption coefficient	0.294 mm^{-1}	
F(000)	1674	
Crystal size	0.120 x 0.100 x 0.100 mm^3	
Theta range for data collection	2.162 to 26.531°.	
Index ranges	-22<=h<=23, -23<=k<=23, -29<=l<=29	
Reflections collected	26733	
Independent reflections	3224 [R(int) = 0.0494]	
Completeness to theta = 25.242°	99.6 %	
Refinement method	Full-matrix least-squares on F^2	
Data / restraints / parameters	3224 / 0 / 120	
Goodness-of-fit on F^2	1.016	
Final R indices [I>2sigma(I)]	R1 = 0.0722, wR2 = 0.2106	
R indices (all data)	R1 = 0.1162, wR2 = 0.2577	
Extinction coefficient	n/a	
Largest diff. peak and hole	0.300 and -0.544 e.Å^{-3}	

References:

1. SAINT Plus; Bruker AXS Inc.: Madison, WI, 2004.

2. L. Krause, R. Herbst-Irmer, G. M. Sheldrick, D. Stalke, *J. Appl. Crystallogr*. 2015, **48**, 3−10.

3. G. M. Sheldrick, SHELXTL, Reference Manual, version 5.1; Bruker AXS Inc.: Madison, WI, 1997.

4. G. M. Sheldrick, *Acta Crystallogr., Sect. A: Found. Crystallogr*. 2008, **64**, 112−122.

5. G. M. Sheldrick, *Acta Crystallogr., Sect. C: Struct. Chem*. 2015, **71**, 3−8.

6. L. Farrugia, WinGX; University of Glasgow: Glasgow, Scotland,2009.

7. A. L. Spek, *Acta Crystallogr., Sect. C: Struct. Chem*. 2015, **71**, 9−18.

8. P. Samanta, A. V. Desai, S. Sharma, P. Chandra and S. K. Ghosh, *Inorg. Chem*., 2018, 57, **5**, 2360–2364.

9.Y.-T. Yan, W.-Y. Zhang, F. Zhang, F. Cao, R.-F. Yang, Y.-Y. Wang and L. Hou, *Dalton Trans*., 2018, **47**, 1682-1692.

10. Y.-T. Yan, F. Cao, W.-Y. Zhang, S.-S. Zhang, F. Zhanga and Y.-Y. Wang, *New J. Chem*., 2018, **42**, 9865-9875.

11. R. Lv, H. Li, J. Su, X. Fu, B. Yang, W. Gu and X. Liu, *Inorg. Chem*., 2017, 56, **20**, 12348–12356.

12. Z. Sun, M. Yang, Y. Ma and L. Li, *Cryst. Growth Des.*, 2017, 17, **8**, 4326–4335.

13. Z. Sun, M. Yang, Y. Ma and L. Li, *Cryst. Growth Des.*, 2017, 17, **8**, 4326–4335.

14. R. Lv, J. Wang, Y. Zhang, H. Li, L. Yang, S. Liao, W. Gu and X. Liu, *J. Mater. Chem. A*, 2016, **4**, 15494-15500.

15. C.-S. Cao, H.-C. Hu, H. Xu, W.-Z. Qiao and B. Zhao, *CrystEngComm*, 2016, **18**, 4445-4451.

16. X.-Y. Guo, F. Zhao, J.-J. Liu, Z.-L. Liu and Y.-Q. Wang, *J. Mater. Chem. A*, 2017, **5**, 20035-20043.

17. J.-J. Zhao, P.-Y. Liu, L.-J. Song, L. Zhang, Z.-L. Liu and Y.-Q. Wang, *Dalton Trans.*, 2021, Advance Article, DOI:10.1039/D1DT00112D.

18. M. Chen, W.-M. Xu, J.-Y. Tian, H. Cui, J.-X. Zhang, C.-S. Liu and M. Du, *J. Mater. Chem. C*, 2017, **5**, 2015-2021.

19. W. Liu, X. Huang, C. Xu, C. Chen, L. Yang, W. Dou, W. Chen, H. Yang and W. Liu, *Chem. Eur.J.*, 2016, **22**, 18769 –18776.

20. G.-X. Wen, M.-L. Han, X.-Q. Wu, Y.-P. Wu, W.-W. Dong, J. Zhao, D.-S. Li and L.-F. Ma, *Dalton Trans.*, 2016, **45**, 15492-15499.

21. J.-N. Hao and B. Yan, *New J. Chem.*, 2016, **40**, 4654-4661.